WSRC-STI-2008-00235
Revision 0

CATALYTIC INTERACTIONS OF RHODIUM, RUTHENIUM, AND MERCURY DURING SIMULATED DWPF CPC PROCESSING WITH HYDROGEN GENERATION

D. C. Koopman

July 2008

E&CPT Research Programs
Savannah River National Laboratory
Aiken, SC 29808

Prepared for the U.S. Department of Energy Under Contract Number DE-AC09-08SR22470

SRNL
SAVANNAH RIVER NATIONAL LABORATORY

DISCLAIMER

Printed in the United States of America

Prepared For
U.S. Department of Energy

WSRC-STI-2008-00235
Revision 0

Key Words: *DWPF, Hydrogen, Noble Metals, Mercury, Catalysis, SRAT, SME*

Retention: Permanent

CATALYTIC INTERACTIONS OF RHODIUM, RUTHENIUM, AND MERCURY DURING SIMULATED DWPF CPC PROCESSING WITH HYDROGEN GENERATION

D. C. Koopman

July 2008

E&CPT Research Programs
Savannah River National Laboratory
Aiken, SC 29808

Prepared for the U.S. Department of Energy Under Contract Number DE-AC09-08SR22470

SRNL
SAVANNAH RIVER NATIONAL LABORATORY
TM

REVIEWS AND APPROVALS

AUTHOR:

D. C. Koopman, Process Engineering Technology Date

TECHNICAL REVIEWERS:

M. E. Stone, Process Engineering Technology Date

R. E. Eibling, Engineering Process Development Date

APPROVERS:

J. C. Griffin, E&CPT Research Programs Manager Date

C. C. Herman, Manager, Process Engineering Technology Date

J. E. Occhipinti, Manager Date
Waste Solidification Engineering

EXECUTIVE SUMMARY

Simulations of the Defense Waste Processing Facility (DWPF) Chemical Processing Cell (CPC) vessels were performed as part of the ongoing investigation into catalytic hydrogen generation. Rhodium, ruthenium, and mercury have been identified as the principal elemental factors affecting the peak hydrogen generation rate in the DWPF Sludge Receipt and Adjustment Tank (SRAT) for a given acid addition. The primary goal of this study is to identify any significant interactions between the three factors. Noble metal concentrations were similar to recent sludge batches. Rh ranged from 0.0026-0.013% and Ru ranged from 0.010-0.050% in the dried sludge solids, while initial Hg ranged from 0.5-2.5 wt%.

An experimental matrix was developed to ensure that the existence of statistically significant two-way interactions could be determined without confounding of the main effects with the two-way interaction effects. The nominal matrix design consisted of twelve SRAT cycles. Testing included: a three factor (Rh, Ru, and Hg) study at two levels per factor (eight runs), two duplicate midpoint runs, and two additional replicate runs to assess reproducibility away from the midpoint. Midpoint testing can identify potential quadratic effects from the three factors. A single sludge simulant was used for all tests. Acid addition was kept effectively constant except to compensate for variations in the starting mercury concentration. Six Slurry Mix Evaporator (SME) cycles were performed to supplement the SME hydrogen generation database.

Some of the preliminary findings from this study include:

- Rh was linked to the maximum SRAT hydrogen generation rate in the first two hours after acid addition in preliminary statistical modeling.
- Ru was linked conclusively to the maximum SRAT hydrogen generation rate in the last four hours of reflux in preliminary statistical modeling.
- Increasing the ratio of Hg/Rh shifted the noble metal controlling the maximum SRAT hydrogen generation rate from Rh to Ru when Ru was at its fission yield ratio to Rh.
- The inhibiting effect of Hg on hydrogen generation apparently does not require much mercury in terms of moles Hg/mole Rh (or Ru). Once the initial impact is realized, the benefit of additional Hg in reducing the hydrogen generation rate was minimal. Sludge Batch 3 and 4 simulant test data confirm this.
- Low Hg runs do not necessarily bound high Hg runs for the maximum hydrogen generation rate over the full SRAT-SME cycle. Two of the four Rh-Ru combinations had a cross-over point where the hydrogen generation rate in high Hg run went from always lower to always higher than in the low Hg run. One cross-over was in the SRAT and one was in the SME. Maximum hydrogen generation rates in the high Hg runs could exceed the maximum hydrogen generation rates from the low Hg runs.
- SME cycle hydrogen generation rates during the first decon canister dewatering period were similar to the rates at the end of the SRAT reflux period.
- Corrosion of 400 series stainless steel shafts significantly impacted the hydrogen generation rate in two runs.

- Preliminary data analysis indicates that several additional SRAT runs are needed to replace suspect data in the original set of twelve runs.

A more detailed statistical evaluation is expected to occur once replacement run data from several additional SRAT runs has been obtained.

TABLE OF CONTENTS

LIST OF FIGURES

LIST OF TABLES

LIST OF ACRONYMS

ACTL	Aiken County Technology Laboratory
AD	Analytical Development
ASP	Analytical Study Plan
CPC	Chemical Process Cell
DWPF	Defense Waste Processing Facility
E&CPT	Environmental and Chemical Process Technology
FAVC	Formic Acid Vent Condenser
GC	Gas Chromatograph
IC	Ion Chromatography
ICP-AES	Inductively Coupled Plasma-Atomic Emission Spectroscopy
ICP-MS	Inductively Coupled Plasma-Mass Spectroscopy
LWO	Liquid Waste Organization
MWWT	Mercury Water Wash Tank
PSAL	Process Science Analytical Laboratory
QA	Quality Assurance
SB	Sludge Batch
SCFM	Standard Cubic Feet per Minute
SME	Slurry Mix Evaporator
SRAT	Sludge Receipt and Adjustment Tank
SRNL	Savannah River National Laboratory
TA	Technical Analyst
TIC	Total Inorganic Carbon
TR	Technical Report
TT&QAP	Task Technical and Quality Assurance Plan
TTR	Task Technical Request
WSRC	Washington Savannah River Company
XAS	X-ray Absorption Spectroscopy

1.0 INTRODUCTION AND BACKGROUND

Due to the greater than expected hydrogen generation during the Tank 51-Sludge Batch 4 (SB4) qualification run, SC-0, DWPF Engineering requested the Savannah River National Laboratory (SRNL) to expand the on-going catalytic hydrogen generation program. The program was designed to increase the understanding of catalytic chemistry in the two major DWPF Chemical Process Cell (CPC) vessels. These are the Sludge Receipt and Adjustment Tank (SRAT) and Slurry Mix Evaporator (SME).

The work presented in this technical report was identified as a result of SRNL/Liquid Waste Organization (LWO) meetings to define potential causes of catalytic hydrogen generation as well as from an external technical review panel commissioned to evaluate SRNL hydrogen related data and programs.[1] The work scope was covered under the technical task request: HLW-DWPF-TTR-2007-0016.[2] A task technical and quality assurance plan (TT&QAP[3]) was drafted to address the needs of the TTR which included issues that were raised in meetings with LWO plus some of the recommendations made by the review panel. A supporting analytical study plan was issued.[4]

The testing discussed in this report focuses on the effects of Rh, Ru, and Hg in a single sludge system with other suspected or known variables held constant. Earlier parts of the hydrogen program indicated a need for this testing. The impact of mercury studies on hydrogen generation in the Sludge Batch 3 (SB3) system indicated a need for follow-up work.[5] The form of noble metal testing showed a correlation between soluble Rh and Ru with hydrogen generation that helped to define a feasible scope for this program.[6,7] These results, along with additional data obtained during SB4 testing, indicated the need for a statistical evaluation of the significance of main factor and two-way interaction effects due to Rh, Ru, and Hg on hydrogen generation. In particular, it was desired to gain a better understanding of the range of conditions where Hg interacts with the noble metal catalysts to inhibit hydrogen generation.

Simulant preparation and preliminary flowsheet studies have been documented.[8] The noble metal and mercury baseline in the preliminary work is summarized in Table 1 along with the ranges covered in the related beaded frit melter feed preparation study that occurred in parallel with the preliminary Rh-Ru-Hg matrix testing.[9]

Table 1. Trim Chemical Ranges

Trim Element	Baseline wt%	Bead-Frit Study wt%
Ag	0.0030	0.0 - 0.20
Pd	0.0010	0.0 - 0.20
Rh	0.0078	0.0 - 0.20
Ru	0.0300	0.0 - 0.375
Hg	1.5000	0.0 - 1.50

The noble metal baseline for the preliminary flowsheet studies became the midpoint case of the Rh-Ru-Hg test matrix. Ag and Pd were fixed at 0.003 and 0.001 wt% in the total solids respectively. Rh, Ru, and Hg were varied from 1/3 to 5/3 of the midpoint values. The Rh and Ru ranges cover measured concentrations of these two noble metals in Sludge Batches 1B through 4. The mercury range was not extended to zero. No DWPF sludge batch is expected to be completely mercury-free. SB3 tests had covered the cases of 0 wt% Hg and 0.11 wt% Hg. It was observed during SB3 and SB4 testing that the maximum hydrogen generation rate increased significantly in the absence of Hg.[5,13] The DWPF SRAT product maximum Hg content is specified as 0.45 wt% Hg. The test matrix range of initial Hg values from 0.5-2.5 wt% in the total solids was chosen to cover an interesting portion of the likely range of DWPF feeds while avoiding the anomalous behavior associated with negligible mercury concentrations.

Prior statistical work found correlations between SRAT hydrogen generation and rhodium.[10] The individual noble metal concentrations were highly correlated by their fission yield ratios. Consequently, the statistical models could not meaningfully distinguish one noble metal from another. The model correlations were effectively between hydrogen and all noble metals simultaneously, rather than with Rh alone. Mercury interaction effects were also found to be statistically significant in some models, typically as an interaction with the noble metals or with various measures of added acid. A statistically significant effect of mercury by itself on the SRAT maximum hydrogen generation rate was not detected in the prior work. Direct comparison tests with both SB3 and SB4 simulants consistently showed a strong inhibiting effect on hydrogen generation when mercury was present versus when mercury was absent. Nitrite ion, as well as SRAT product nitrate which can reflect nitrite-to-nitrate conversion, also appeared in some of the statistical models.

Previous statistical work also failed to find a correlation between the maximum hydrogen generation rates in the SRAT and SME cycles.[10] A significant lack of correlation between the two maximum rates was indicated. Additional data are needed to help with the understanding of SME cycle hydrogen rates and how they relate to the SRAT results. Half of the tests in this study had Rh/Ru at the appropriate fission yield ratio of 1/3.75. SME cycles were performed on these six runs to expand the data base of SRAT-SME simulations producing relatively significant hydrogen. The other six tests had ratios set by the constraints of a full factorial statistically designed test matrix. Rh and Ru were at the fission yield ratio were when they were either both low or both high.

The Rh-Ru-Hg matrix testing was not expected to produce hydrogen above the scaled equivalent to the DWPF design bases of 0.65 lbs/hr in the SRAT and 0.223 lbs/hr in the SME. It was anticipated, however, that hydrogen generation rates could approach the DWPF limits when Rh and/or Ru were at their maximum values based on the data from the preliminary flowsheet tests at the midpoint concentrations.

2.0 APPROACH

2.1 Structure and Objectives of Test Program

Twelve CPC simulations were performed using the 4-L SRAT-scale equipment at Aiken County Technology Laboratory (ACTL). The twelve 4-L simulations were given the Rh, Ru, and Hg loadings and run identifiers listed in Table 2. Nominal Hg levels were 0.5, 1.5, and 2.5 wt%. Nominal Ru levels were 0.01, 0.03, and 0.05 wt%. Nominal Rh levels were 0.0026, 0.0078, and 0.013 wt%. Individual wt%'s in Table 2 differed slightly from the nominal targets due to the impact of dilution from the other two trim chemicals.

Table 2. Test Matrix for Simulations

Run	Position	Rh, wt%	Ru, wt%	Hg, wt%
RhRuHg1	L-L-L	0.00263	0.01012	0.506
RhRuHg2	H-L-L	0.01315	0.01012	0.506
RhRuHg10	L-H-L	0.00263	0.05056	0.505
RhRuHg4	H-H-L	0.01314	0.05054	0.505
RhRuHg5	L-L-H	0.00257	0.00990	2.475
RhRuHg6	H-L-H	0.01287	0.00990	2.474
RhRuHg7	L-H-H	0.00257	0.04948	2.472
RhRuHg8	H-H-H	0.01285	0.04946	2.472
RhRuHg9	M-M-M	0.00780	0.03000	1.500
RhRuHg11	M-M-M	0.00780	0.03000	1.500
RhRuHg12	H-L-L	0.01315	0.01012	0.506
RhRuHg13	H-L-H	0.01287	0.00990	2.474

The first nine rows of Table 2 constitute a full factorial designed experimental matrix on three factors at two levels plus a midpoint. The position column indicates whether the factors Rh, Ru, and Hg respectively were at low (L), high (H), or midpoint (M) levels. Conceptually, the SRAT tests were laid out per Figure 1 in the form of a cube with tests at each of the eight corners of the cube along with the center of the cube.

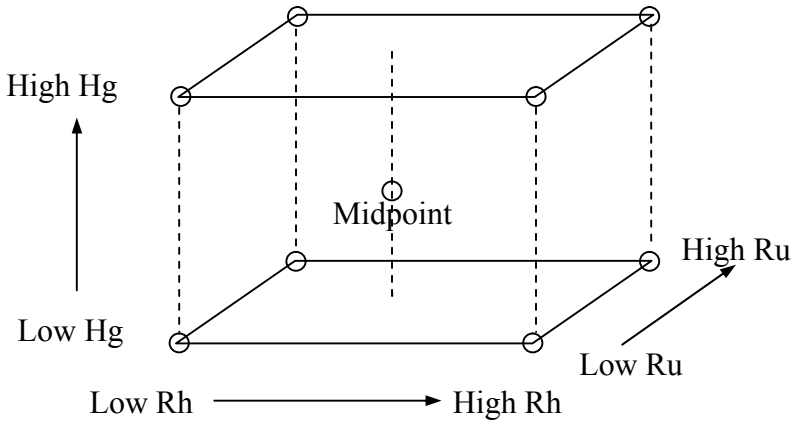

Figure 1. Structure of Rh-Ru-Hg test matrix

The full factorial design supports statistical modeling for main (single factor) effects from Rh, Ru, and Hg as well as for pair-wise interactions and non-linearity. Three replicate runs were recommended for inclusion into the statistical design, at least one of which had to be the midpoint test. The tests were not run in numerical order. The final choices for the two replicates, RhRuHg12 and 13, were made in order to evaluate the relative magnitude of unexpected factors that occurred during RhRuHg2 and 6 respectively. These will be discussed in Section 3.0.

The two midpoint runs were nearly replicates of H2Sim4, one of the preliminary flowsheet runs.[8] The only difference was a small shift in the ratio of formic acid to total acid which was 0.932 in H2Sim4 and was 0.913 in RhRuHg9 and 11. Test RhRuHg3 (not in the table) was replaced with run RhRuHg10 when the GC failed in RhRuHg3.

All tests had 2,900 g of starting sludge (before trim chemicals and rinse water). The actual masses of a given trim chemical added at a given level were always identical. Rh was trimmed as a 4.93 wt% rhodium solution of $Rh(NO_3)_3$. Ru was added as the dry trivalent chloride salt at a purity of 41.73 wt% Ru. Pd was trimmed as a 15.27 wt% palladium solution of $Pd(NO_3)_2$. Silver was added as the dry nitrate salt $AgNO_3$. Mercury was trimmed as dry HgO. Yellow HgO was used in most tests. Yellow HgO is a finer particle than red HgO. Chemically, the two are the same. Red HgO was used in three of the high Hg concentration runs, RhRuHg5-RhRuHg7, because there was no yellow HgO.

2.2 Chemical Process Cell Simulation Details

Simulated DWPF washed sludge was prepared for the catalytic hydrogen generation program by blending available generic A, B, and C sludge simulants.[8] An average composition based on nine independent samples of the simulant prior to the Rh-Ru-Hg matrix study is given in Table 3 for the elements after calcining at 1100°C. These were determined by inductively coupled plasma-atomic emission spectroscopy (ICP-AES).

Table 3. Wt% Calcined Elemental Composition of Sludge

	ABC Blend Simulant wt%
Al	16.0
Ba	0.21
Ca	2.50
Cr	0.15
Cu	0.10
Fe	21.5
K	0.19
Mg	1.5
Mn	3.9
Na	12.7
Ni	0.87
Pb	0.047
Si	1.62
Ti	0.019
Zn	0.20
Zr	0.44

Table 4 gives corresponding density and solids data. The wt% total solids were measured on the slurry. The wt% dissolved solids were measured on the filtered supernate (no insoluble solids). These two measured values were used to calculate the wt% soluble and insoluble solids of the slurry.

Table 4. Density and Solids Data on Blend Simulant

	ABC Blend Simulant
Wt% total solids	22.8
Wt% insoluble solids	16.8
Wt% soluble solids	6.0
Wt% calcined solids	16.0
Slurry Density, g/mL	1.175
Supernate Density, g/mL	1.053

Table 5 summarizes the available information on total anions in the simulant slurry. Values are mg indicated species per kg of the untrimmed simulant slurry. Results come from a variety of analytical and computational methods. Ion chromatography (IC) is the preferred analytical method, but some species which were added to the simulant fell below the instrument detection limits. Anions, such as oxide, phosphate, and oxalate, are not necessarily present as dissociated species.

Table 5. Anion Data on Blend Simulant Slurry

ABC Blend Simulant	mg/kg
OH^- (by ion-mass balance)	80,000
NO_2^-	17,950
NO_3^-	10,850[1]
O^{2-} (by ion-mass balance)	13,000
$C_2O_4^{2-}$ (by recipe calculation)	1,400
PO_4^{3-} (by ICP P)	160
SO_4^{2-} (by IC)	1,625
SO_4^{2-} (by ICP S)	1,350
Total Inorganic Carbon	849[2]
Cl^-	390
F^- (by recipe calculation)	47

1 – revised to 13,790 mg/kg later
2 – revised to 1,350 mg/kg later

A simulant preparation recipe calculation gave the fluoride and oxalate values in Table 5. Phosphate was below the detection limit by IC, so it was calculated from the slurry ICP-AES value for phosphorous (a measure of total phosphate rather than soluble phosphate). Total sulfate, calculated from ICP-AES sulfur, was somewhat less than sulfate by IC. The two values can be reconciled if one is 10% high and the other is 10% low. Sulfur can also be partially volatilized and lost during high temperature sample preparations. The simulant slurry was titrated using the ACTL auto-titrator to pH 7. The average result was 0.313 M equivalent hydroxide.

Subsequent sample data and analysis supported a nitrate value of about 13,800 mg/kg and a total inorganic carbon value (TIC) of 1,350 mg/kg. The OH^- and O^{2-} content of the slurry were set by difference using an ion mass balance that accounted for the remaining positive charge in the simulant cations after totaling the measured anions while simultaneously achieving consistency in the wt% solids data (100% OH^- and 0% O^{2-} would exceed the allowable solids mass, while the reverse case would not produce sufficient solids mass; the ion balance finds an intermediate point that satisfies both criteria; the split is subject to uncertainties in the other anion concentration values, but these account for only 12% of the total negative charge, so the downstream impact of their uncertainties on the calculation is expected to be relatively minor).

The trimmed SRAT receipt volume was about 2.5 L. One acid calculation was used for all runs at a given Hg level. Adjustments for changes in Hg level were made at one mole acid added per mole Hg added, and this acid increment was not multiplied by the stoichiometric correction factor. Formic acid made up about 91.3% of the total acid. A stoichiometric factor of 204.5% was chosen based on the preliminary acid window study.[8] This factor led to an acid addition of 2.067 moles acid per liter of untrimmed simulant at the midpoint Hg concentration. These acid levels were about 5% larger than the bead-frit study (198% and 1.96 moles acid/L).

Nominal scaled DWPF SRAT/SME processing conditions were generally used; however, neither cycle had a heel from a prior batch.

- The SRAT air purge scaled to 230 scfm in DWPF.
- A 200 ppm antifoam addition was made prior to nitric acid addition.
- A 100 ppm antifoam addition was made prior to formic acid addition.
- Nitric and formic acid addition were at 93°C.
- Acid was added at two gallons per minute scaled from 6,000 gallons to 2.5 L.
- A 500 ppm antifoam addition was made prior to going to boiling following acid addition.
- Boiling targeted the scaled 5,000 lbs/hr at DWPF scale.
- SRAT dewatering typically took about 50 minutes.
- Reflux followed dewatering. The end of the 12-hour reflux period defined the end of the SRAT cycle.
- After SRAT product samples were pulled, the air purge was adjusted to the scaled SME rate, 74 scfm.
- A 100 ppm antifoam addition was made at the start of the SME.
- Two canister decon dewaterings followed at the scaled equivalent of 1,000 gallons water per canister decon added and boiled off.
- Two frit-water-formic acid slurry additions targeting 35% sludge oxides came after the final canister decon with associated dewaterings.
- After the second frit-water-formic acid slurry addition dewatering, the SME was concentrated to 50 wt% total solids.

A complete SRAT/SME simulation took about 36 hours measured from the start of heating prior to acid addition in the SRAT until the time that the SME product had cooled to less than 50°C. Simulations were run continuously except for a short break between the SRAT and SME cycles.

2.3 Process and Sample Analytical Methods

The automated data acquisition system developed for the 4-L SRAT rigs was used to collect electronic data on a PC. Data included SRAT temperature, bath temperatures for the cooling water to the SRAT condenser and Formic Acid Vent Condenser (FAVC), slurry pH, SRAT mixer speed and torque, air and helium purge flows (He is used as an internal standard and is set to 0.5% of the nominal SRAT or SME air purge flow), and raw GC data. Cumulative acid addition volume data were collected from the automated dispensers using an algorithm that virtually matches the indicated total on the dispenser (the dispenser total is not available in the outlet data stream from the device). All of the tests had a pH probe in the SRAT slurry to monitor pH. Performance of this lot of pH probes was problematic and included many outright failures.

Agilent 3000A micro GC's were used on all twelve runs. Column-A can collect data related to He, H_2, O_2, N_2, NO, and CO, while column-B can collect data related to CO_2 and N_2O. GC's were calibrated with a standard gas containing 0.499 vol% He, 1.010 vol% H_2, 20.00 vol% O_2, 51.0 vol% N_2, 25.0 vol% CO_2 and 2.50 vol% N_2O. Room air was used to give a two point calibration for N_2. The GC's were checked with calibration gas following the SRAT cycle and again following the SME cycle. NO vol% data were obtained semi-quantitatively using the historical ratios of He/NO area factors for the individual GC's, since no calibration gas with NO

was available. No evidence for CO generation was obtained while examining the region of the chromatogram where it would elute.

The GC's were baked out between runs. The inlet GC samples passed through small sintered metal filters prior to injection into the two columns. Selected ranges of GC raw data were reprocessed in order to obtain the best correlations between peak areas and volume percents and to correct for any periods where peaks were not properly identified and integrated. The main issue was one of proper peak identification when a gas showed up for the first time during processing. One of the twelve runs, RhRuHg8, had an apparent drift in hydrogen calibration of about 10% during the SRAT. This drift is at the limit where data are considered acceptable. The GC's drifted less than 4% in the other eleven SRAT cycles, so hydrogen comparisons can be made to within 8% between two runs. Furthermore, eleven of the twelve drifts in hydrogen calibration were in the same direction, so effects of drift tended to cancel out when comparing runs. No other significant GC issues were noted during the runs.

The reproducibility of off-gas data from run to run, particularly in the form of the DWPF-scaled hydrogen generation rate, appears to be larger than can be explained based solely on the uncertainties in the GC vol% data and helium mass flow controller calibrations. The relative hydrogen uncertainties in many cases should put replicates within about ~5%, but the historical reproducibility of repeated trials suggests something in the 20-40% range. Pairs of runs performed at the same time seem to be more consistent than pairs of runs performed at different times. The current hypothesis is that small variations in the reactions occurring prior to hydrogen generation contribute to an increased lack of reproducibility. The 4-L tests are more tightly controlled with respect to acid flowrates and timing than the 22-L tests where much of the comparable run pair data were found. For these reasons the smaller tests are expected to be comparable toward the lower end of the reproducibility range, or 20-30%. This range includes the effect of GC calibration drift and potential bias between different He mass flow controllers. Pairs of runs that shared the same helium MKS mass flow controller and had minimal GC calibration drift should be more directly comparable with smaller potential reproducibility issues. Uncertainty will refer to measurement uncertainty effects (H_2 and He vol% and flow rates) while reproducibility will refer to historical limits in the discussion in Section 3.0.

Process samples were analyzed by various methods. Slurry and supernate elemental compositions were determined by ICP-AES at the Process Science Analytical Laboratory (PSAL). Slurry samples were calcined at 1100°C, however, so that the noble metals, Pb, and Cr were underreported. These species have shown significant loss during the calcining/dissolution preparation in the past. ICP-AES data are not used to track these species. Soluble slurry anions were determined by IC on 100-fold weighted dilutions of slurry with water after filtering out insoluble solids. Selected SRAT product slurry samples were submitted to Analytical Development (AD) for ICP-Mass Spectroscopy (ICP-MS) analysis for Pd, Rh, and Ru. SRAT products were checked for mercury content by AD. Condensates from the MWWT and FAVC were analyzed for anions as part of the program to better characterize SRAT chemistry.

2.4 DWPF-Scale Hydrogen Generation Rate Calculation

DWPF-scale hydrogen generation rates were calculated from the H_2/He vol% ratio, known He flow, and the scale factor for the tests. Helium flow was controlled by an MKS mass flow controller. The hydrogen generation rate at DWPF scale was calculated as follows:

$$H_2, DWPF\ lbs/hr = \frac{vol\%\ H_2}{vol\%\ He} * \frac{std\ cm^3\ He}{minute} * \frac{2.016\ g\ H_2/mole}{22{,}415\ std\ cm^3/mole} * \frac{60\ min/hr}{453.6\ g/lb} * scale\ factor$$

SRAT cycle He flow was generally close to 3.67 standard cm^3 per minute (sccm) and the scale factor was close to 8,800. The He flowrate was generally close to 1.0 sccm and the scale factor was close to 10,000 for the SME cycle. Parameter variations between runs were larger in the SME cycle due to variations in the mass of samples removed during the SRAT cycle. Similar calculations can be performed on the other gases.

This page intentionally left blank.

3.0 SRAT/SME DATA DISCUSSION

Section 3.0 presents results from the twelve SRAT cycles and six SME cycles. The midpoint SRAT data for the baseline case are presented first. SRAT data from the other eight starting compositions constitute perturbations away from the midpoint data. Instead of giving eight sets of individual results for the eight Rh-Ru-Hg combinations away from the midpoint, the effect of mercury will be emphasized initially. Data will be given for each of the four different high/low Rh-Ru combinations with both the high and low Hg results plotted together to show the impact of Hg graphically. Discussion of SME data follows the SRAT data.

3.1 Comparison of SRAT Data from Matrix Test Pairs

3.1.1 Midpoint (Baseline) Composition Results

The midpoint results were expected to be similar to the preliminary test called H2Sim4 from the simulant flowsheet tests.[8] These three tests had identical noble metal and mercury loadings and overall acid addition in terms of moles acid added per liter starting sludge. Only the ratio of formic acid to total acid differed slightly: 0.932 in H2Sim4 versus 0.913 in the matrix.

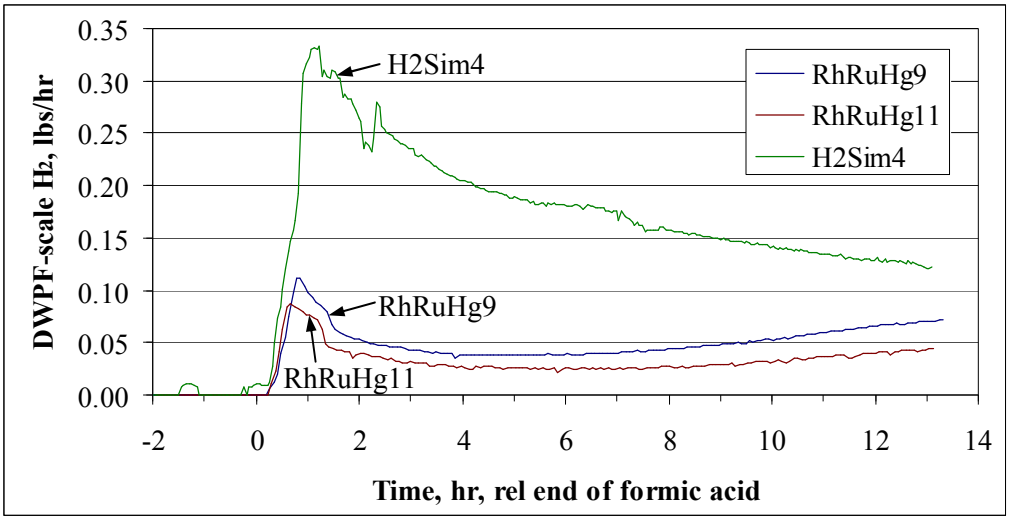

Figure 2. Midpoint hydrogen results

Hydrogen data for the two matrix midpoint tests, RhRuHg9 and RhRuHg11, agreed very well with respect to event timing. They were generally both rising or falling at the same time, but the quantitative agreement was only about 70% on the peak hydrogen generation rate and 55% at the end of the SRAT. Factor of two differences persisted through the SME cycle. These differences are larger than expected in replicate runs and may suggest that some process parameter was inadvertently varied between the two runs.

H2Sim4 hydrogen generation rates were very different from the midpoint matrix runs. H2Sim4 hydrogen generation rates were more than double that of either matrix run over nearly the entire

period of significant hydrogen production from 0.5-13 hours after acid addition. H2Sim4 data were given additional scrutiny after analyzing the new hydrogen data. It was noted that the MWWT was inadvertently drained during dewatering following formic acid addition, and that consequently H2Sim4 was probably not as equivalent to the matrix runs as it should have been following the start of reflux at about +1.3 hours. The peak hydrogen generation rate, however, occurred just before the start of reflux, so this major peak difference between the runs cannot be explained by the prematurely drained MWWT. The inadvertent MWWT draining may explain why H2Sim4 hydrogen generation rates continuously fell during reflux while the matrix tests fell and then began rising again after 3-4 hours of reflux.

The only identified difference in H2Sim4 at the time of the peak hydrogen generation rate was the higher formic acid/total acid ratio. This ratio was not that different from the matrix midpoint runs, but it did produce a 22% increase in total nitric acid addition. This in turn may have altered nitrite destruction kinetics and affected the catalytic activity of a nitro-rhodium complex catalyst. If so, the behavior is different from the SB2-3 process variability study results.[11] The targeted redox was adjusted in that testing to cover 0.0, 0.1, and 0.2 $Fe^{2+}/\Sigma Fe$. Formic acid to total acid ranged from 0.82 to 0.94. This is a wider range than between H2Sim4 and the midpoint runs, and it includes the current range (no extrapolation). No difference in hydrogen generation rates were seen in that study as the redox target changed. The testing, however, was at 0.117 wt% initial Hg, which lies well below the Rh-Ru-Hg matrix range. This 13-fold reduction in Hg could be a factor in the results. The Rh-Ru-Hg matrix study was partly developed to determine the significance of Hg in a broader context than past work. The current understanding of hydrogen generation and SRAT data reproducibility do not explain the differences between H2Sim4 and the midpoint runs.

The H2Sim4 results are consistent with the other preliminary flowsheet test results, i.e. H2Sim4 does not appear to be outlier data in the context of the other three flowsheet runs. The midpoint runs also replicated themselves fairly well. One possibility is that the May 2007 sludge simulant used in all three of the tests changed with storage time such that the acid demand increased. H2Sim4 was run 6/6/07, RhRuHg9 was run 10/29/07, and RhRuHg11 was run 3/24/08. Hydrogen generation rates were lower each time the simulant was used at the midpoint conditions. The biggest change occurred between 6/6 and 10/29.

Results from the sixteen run bead-frit study showed only mild variations in hydrogen generation within each of the eight pairs. These variations were of similar relative magnitude to those between the two midpoint runs. The first bead-frit tests started a month after H2Sim4 and completed in November 2007, however, so there were no data in that block with simulant as fresh as in H2Sim4. Therefore, if the simulant acid demand did change with time, it must have made the largest change between when it was first prepared and the initial bead-frit study runs (between May and July) with only relatively small changes afterwards in order to be consistent with all of the available data. The auto-titration of the simulant to pH 7 held constant over fourteen months (5/07-8/08), so any change was probably in the relative reactivity of the insoluble hydroxides which does not show up in the titration. Chemistry of the insoluble solids is difficult to track since the routine chemical analyses performed on sludge simulants are not sensitive to speciation and surface chemistry of the solids.

Although the three tests with midpoint trim concentrations occurred at different times of the year, this did not have a large impact on the CO_2 data. Replication of the CO_2 data was generally good across all three runs as seen in Figure 3 except near -3.5 hours where the data was impacted by the variable down time required to switch from nitric acid feed to formic acid feed. Data were generally within ±10% except for select individual GC readings. The time axis was expanded to show the period of acid addition, dewatering, and maximum CO_2 production. The expanded scale tends to emphasize the random variations from injection to injection to the GC compared to the 18-20 hour scales for the full SRAT cycle.

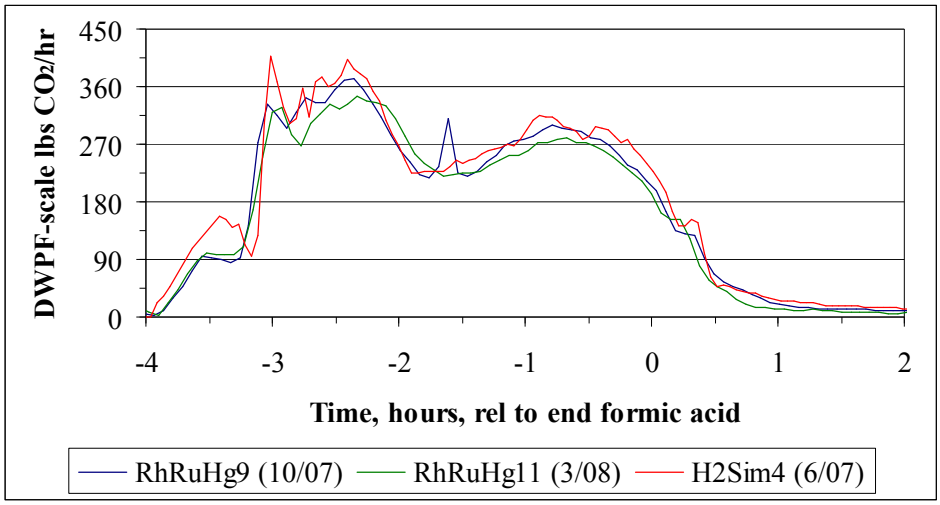

Figure 3. Midpoint CO_2 results

The matched timing of the declining CO_2 just before and after the end of acid addition indicates that all three runs were following similar acid additions. Consequently, the enhanced hydrogen rates in H2Sim4 do not appear to be due to a larger than expected acid addition. If they were, the red line for H2Sim4 CO_2 in Figure 3 would be shifted to earlier times than the lines for the two matrix runs, and this is not the case. The CO_2 data do not seem to indicate a major aging effect on the acid demand of the sludge simulant. An increase in acid demand would tend to shift the decay in CO_2 production that started at about -0.5 hours to the right. GC samples were taken once every 4.0-4.5 minutes. Some sample-to-sample variations seem to be more extreme than others, e.g. the RhRuHg9 point at -1.6 hours, however examination of the full chromatogram data indicates that excessive sample was injected in this instance giving rise to inflated readings for all components.

The RhRuHg11 CO_2 trace was alternately above and below the RhRuHg9 trace, but integrated total production of CO_2 in RhRuHg9 was about 7% higher than RhRuHg11 for the SRAT cycle. This suggests that there was not a major impact on the mass flowrate calculations from bias in the He internal standard flowrate. The higher CO_2 also suggests that RhRuHg9 was more catalytically active than RhRuHg11, but the difference is close to the measurement uncertainty. This in turn supports the hypothesis that the hydrogen differences were primarily ones of reproducibility rather than of measurement uncertainty.

The N_2O results seem to indicate that nitrite destruction chemistry did occur differently in H2Sim4 than in the two matrix runs. Figure 4 shows the N_2O production rates at DWPF scale for the three runs.

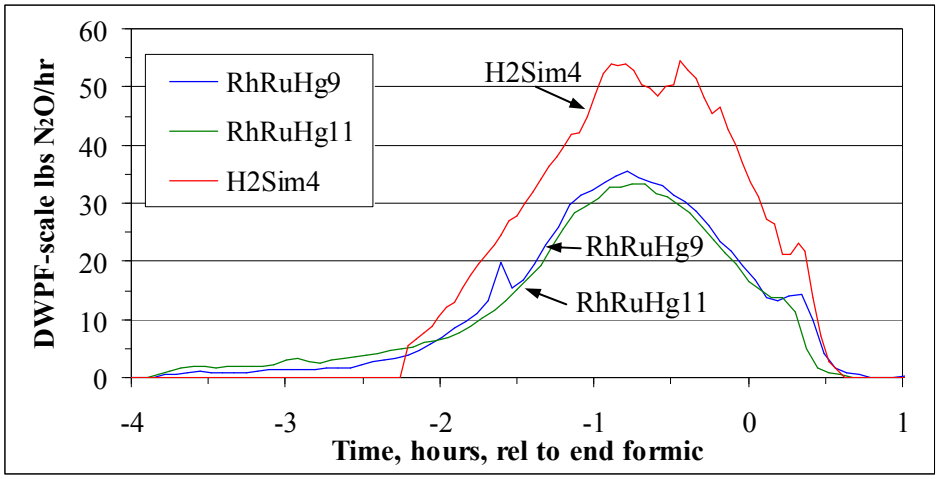

Figure 4. Midpoint N_2O results

The N_2O data indicate that something promoted N_2O formation in H2Sim4 relative to the matrix runs. N_2O production was generally found to increase as the initial mercury concentration decreased during the Rh-Ru-Hg matrix study. The midpoint data could be interpreted as indicating that only a fraction of the targeted mercury content participated in the usual reactions in H2Sim4 compared to the two matrix runs. A drop in mercury concentration would be likely to promote increased hydrogen generation rates based on results from testing with earlier sludge batch simulants.

3.1.2 Low Rh-Low Ru Results

The impact of high and low levels of mercury on the hydrogen generation rate profiles at 0.00267% Rh and 0.010% Ru is shown in Figure 5.

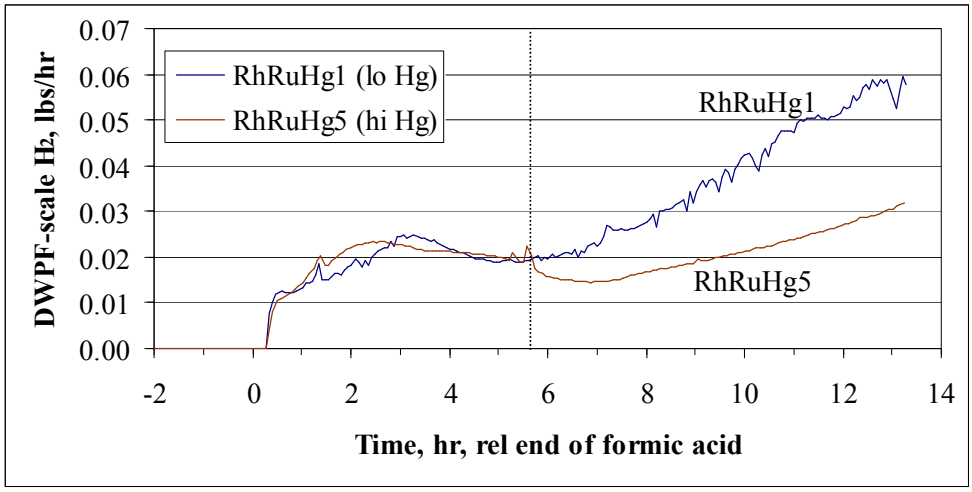

Figure 5. Hydrogen at low noble metal concentrations

The surprise in these data was that the two profiles were nearly identical until six hours after the end of formic acid addition in spite of the five-fold mercury difference. The inhibiting effect of mercury was close to the noise level of the data. (GC drift was minimal in both runs, and both runs used the same He MKS flow controller.) The similarity in hydrogen generation rates was unlike what was seen in SB3 tests going from no mercury to 0.11% Hg.[5] It was also unlike what was seen in Sludge Batch 4 (SB4) data going from 0-1 wt% Hg.[12] Apparently, the inhibiting effect of mercury on hydrogen generation does not require much mercury in terms of moles Hg/mole Rh (or Ru), but once the initial impact is realized, the benefit of additional Hg in reducing hydrogen generation is minimal. The results may have been impacted by the use of red HgO in RhRuHg5.

Maximum hydrogen generation rates came at the end of the SRAT rather than shortly after acid addition. The timing suggests Ru was the major catalyst controlling the peak generation rate, not Rh. Preliminary statistical modeling of the matrix data supports this hypothesis. RhRuHg5 actually passed RhRuHg1 in terms of hydrogen generation in the SME cycle, Section 3.3.1. Therefore, the low Hg run did not bound the behavior of the high Hg run in terms of hydrogen generation over the entire SRAT plus SME cycles. Data for CO_2 were examined for various reasons including to check on the consistency of acid addition timing. Data for the two low noble metal runs are shown in Figure 6.

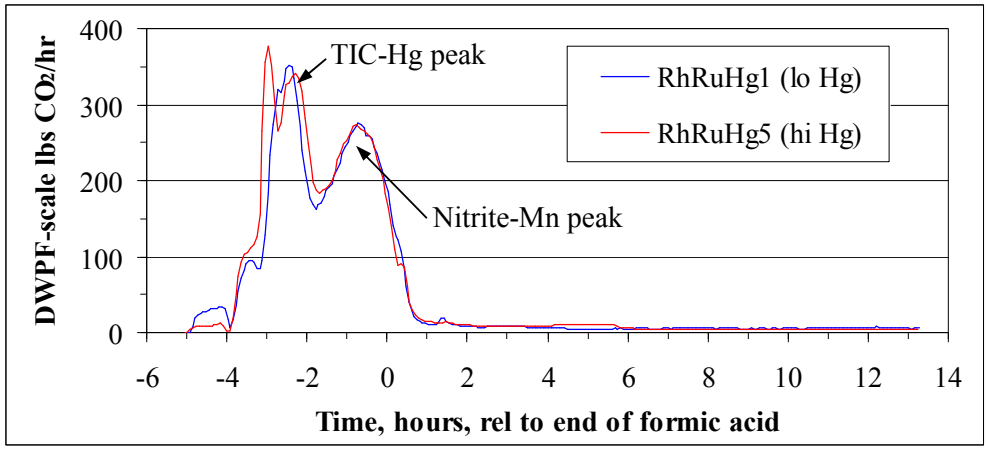

Figure 6. CO_2 at low Rh-low Ru

The peak at -0.7 hours is the nitrite-Mn reduction peak where formic acid converts to CO_2. The near simultaneity of these two peaks at two Hg levels is expected for practically identical acid additions. It confirms that both acid additions delivered the targeted volumes, and tends to confirm that one extra mole of acid per extra mole of Hg was the correct adjustment. The difference in area under the overall SRAT CO_2 profiles at lab-scale was 3.3 g out of slightly more than 50 g total production. An increase of 2.95 g of CO_2 was expected from reduction of 0.067 moles of additional Hg^{2+} in the high Hg run. The expected and measured total CO_2 mass differences were surprisingly consistent for this pair.

The N_2O data for the two runs are given in Figure 7.

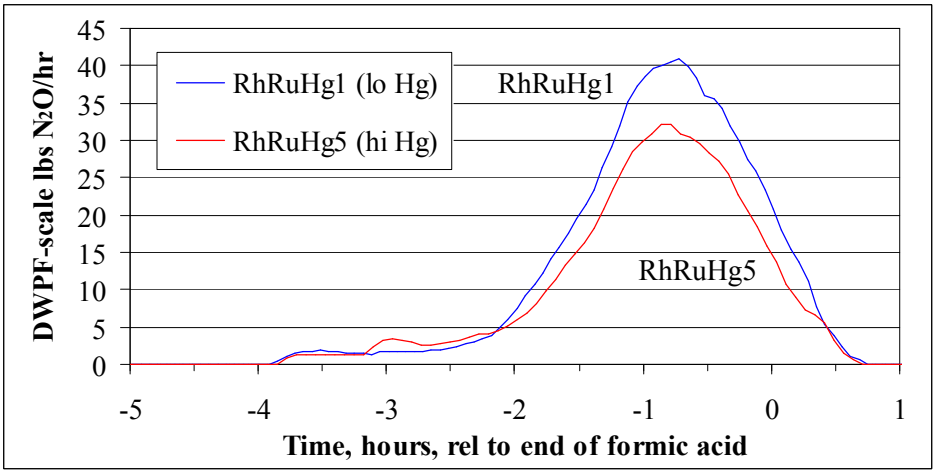

Figure 7. N_2O at low Rh-low Ru

Increased initial mercury seemed to inhibit N_2O production. The two midpoint Hg cases peaked at about 34.5 lbs/hr, or in between the high and low Hg cases here. This supports the trend of N_2O suppression with increasing Hg. An even larger drop was seen in the bead-frit tests between two runs with 0.2 wt% Ru and no Hg (~90 lbs/hr peak), and one run with 0.2 wt% Ru

and 1.5 wt% Hg (~10 lbs/hr peak).[13] (These three bead-frit program tests had no Rh or Pd. Rh and Pd were both found to catalyze formation of N_2O.) The drop in N_2O production had the potential to cause a matching drop in CO_2 production unless catalytic reduction of nitrite to NO by formic acid made up the difference (which seemed to be the case here).

3.1.3 Low Rh-High Ru Results

The impact of high and low levels of mercury on the hydrogen generation rate profiles at 0.00267% Rh and 0.050% Ru is shown in Figure 8.

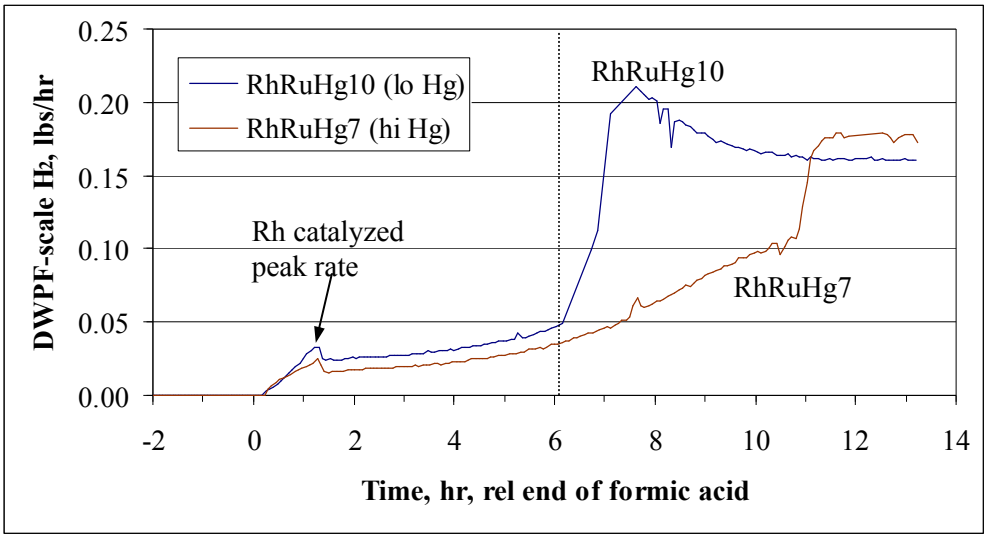

Figure 8. Hydrogen at low Rh-high Ru

The two hydrogen generation rate profiles were very similar for about six hours after the end of formic acid addition. The run with less Hg generally had a 20-40% higher generation rate which is close to the range of reproducibility of the results (the GC during RhRuHg10 drifted up 3%, while the GC during RhRuHg7 drifted down 2% in addition to relative uncertainty in the helium flowrates used to convert hydrogen compositions to flowrates; two different MKS flow controllers were used to set the He flow in the two runs). The measured Rh driven peak hydrogen generation rate at ~1.2 hours after formic acid was only reduced 15% from increasing initial mercury by a factor of five. RhRuHg10 was trimmed with yellow HgO, while RhRuHg7 was trimmed with the red HgO, but it is not clear that this had any significant impact on the hydrogen data.

The general hydrogen generation behavior was similar to the low Rh-low Ru combination. The maximum hydrogen generation rates came relatively late in the SRAT, suggesting that the high Ru content dominated over the low Rh content in controlling the peak magnitude and timing. The variation, however, was more pronounced with higher Ru than in the low Rh-low Ru pair. As the ratio of added Hg/Rh increased, the tendency was to shift the peak hydrogen generation rate into the later Ru-dominated period of the SRAT.

The CO_2 data for this pair of runs are given in Figure 9.

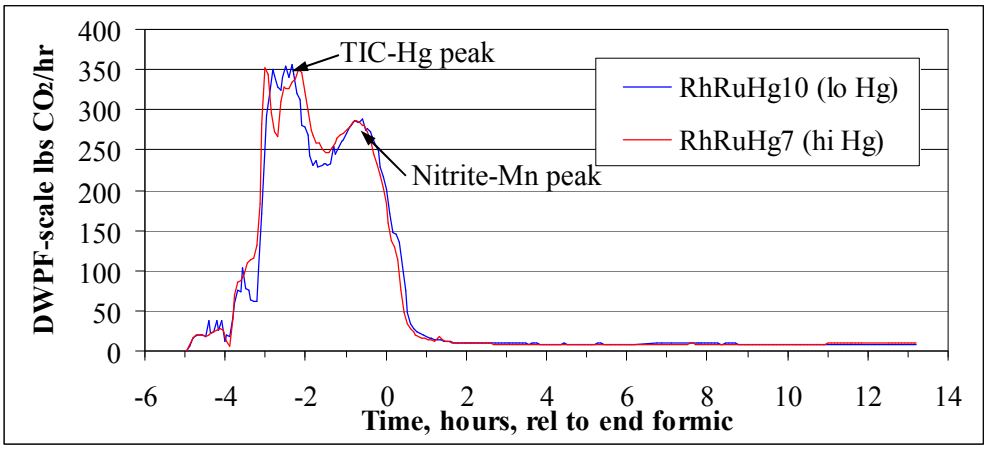

Figure 9. CO_2 at low Rh-high Ru

Alignment of the two nitrite-Mn reduction peaks was excellent confirming acid addition volumes were close to target. The high Hg run produced 59.2 g CO_2 versus 58.2 g in the low Hg run. The delta is less than the 2.95 g expected from the additional Hg, but the difference could be caused by changes in other reactions producing CO_2 during other parts of the SRAT cycle. Corresponding data for N_2O are given in Figure 10.

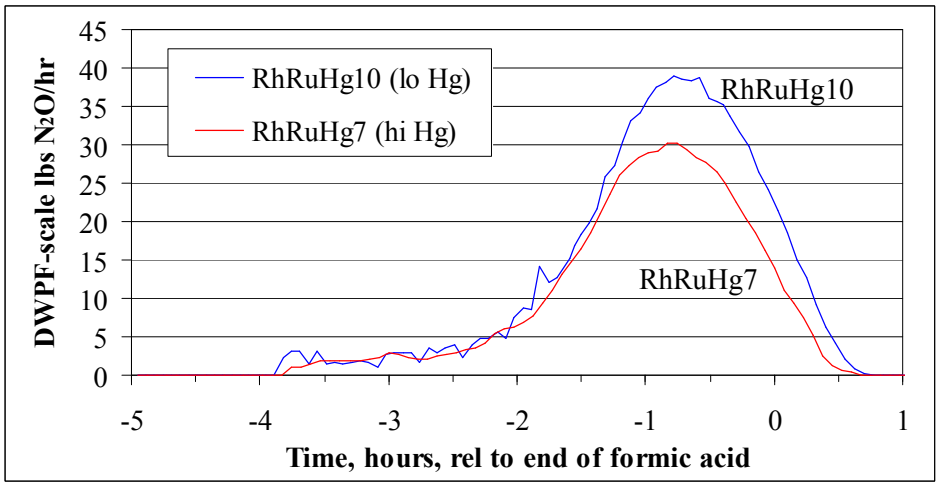

Figure 10. N_2O at low Rh-high Ru

The N_2O generation rate profiles were fairly similar to those for low Rh-low Ru. The low Hg case peaked slightly higher than the high Hg case in both pairs. Peaks were in the 30-40 lbs/hr range at DWPF scale for both pairs (~2 vol% versus ~1.5 vol%). The two low Rh-high Ru curves bracketed the midpoint cases at 34.5 lbs/hr on average, supporting an inhibiting effect of higher Hg concentrations on N_2O production.

3.1.4 High Rh-Low Ru Results

The impact of the high and low levels of mercury on the hydrogen generation rate profiles at 0.0133% Rh and 0.010% Ru is shown in Figure 11. These four runs all used a different He mass flow controller. RhRuHg6 had nearly a 4% drift in hydrogen calibration during the run while the other three stayed closer to the initial calibration.

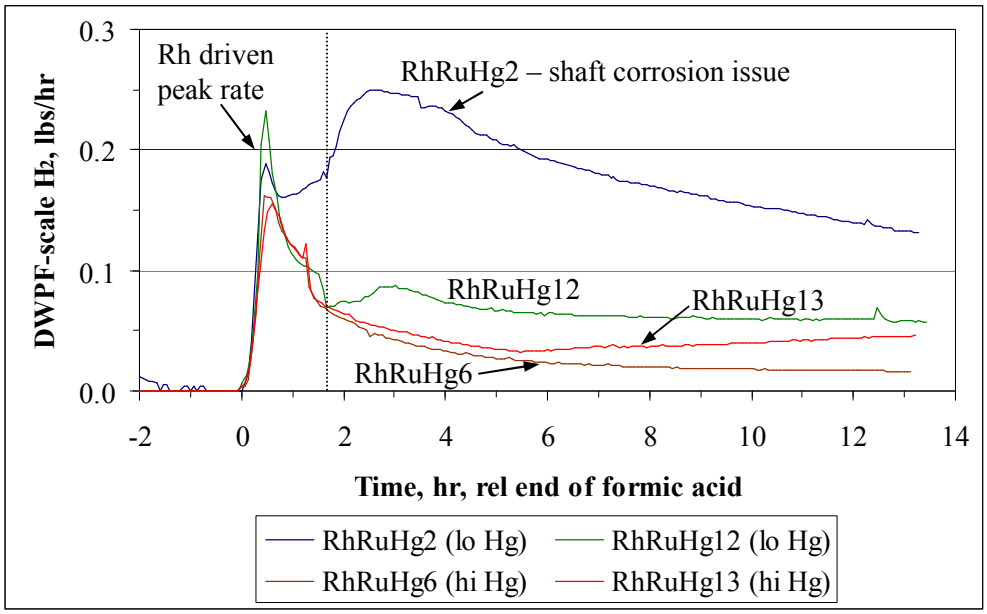

Figure 11. Hydrogen at high Rh-low Ru

RhRuHg2 and RhRuHg6 were selected as the low Hg and high Hg case to perform replicate measurements to support the preliminary statistical analysis of the data. The two choices were not arbitrary. RhRuHg2 (above) and RhRuHg4 (in Section 3.1.5) simulations accidentally used new agitator shafts made from a 400 series stainless steel clad section of bar stock. The core stock was exposed at the bottom end creating an electrochemical cell between the core and the cladding through the sludge supernate. Extreme corrosion of the shafts occurred in these two runs. This was visually obvious. Statistically significant increases in the supernate Cr and Fe concentrations were also found in the SRAT product of these two runs compared to the other ten matrix study runs. These higher concentrations were interpreted to be due to corrosive dissolution of these elements in the stainless steel.

The hydrogen generation rate data that RhRuHg12 clearly did not replicate RhRuHg2 as intended. The main difference was the sustained high generation rates in RhRuHg2 from two hours after the end of formic acid addition until the end of the SRAT. This additional hydrogen was tentatively attributed to the byproduct of acidic corrosion that dissolved metal in the shaft. Oxidation of metallic elements by aqueous acids is generally accompanied by reduction of acid protons to hydrogen. These reactions do not produce CO_2 with the H_2, and no excess CO_2 was noted during the period of increased hydrogen generation. The two low Hg run peaks at +0.5 hours were not too dissimilar. Both low Hg runs peaked higher at 0.5 hours than the two high Hg runs. This trend was the pre-run expectation.

RhRuHg2 had a second issue when it was inadvertently dewatered about 90 g past the 253 g target. This was noticed at the end of dewatering. A dilute solution of approximately 80 g of de-ionized water and 9 g of composite dewatering condensate was added back to the SRAT to reestablish nominal concentrations in the slurry about fifteen minutes later. The composite dewatering condensate cannot accurately represent the composition of fresh condensate due to moderately rapid reactions, e.g. nitrite-to-nitrate conversion, that occur in the MWWT and Slurry Mix Evaporator Condensate Tank (composite condensate collection bottle). Data after the run indicated that there was probably a net loss of formate ion/formic acid in RhRuHg2 from excess dewatering. This loss would be expected to negatively impact hydrogen generation based on small formic acid additions normally enhancing hydrogen generation in the SME cycle. In spite of this, RhRuHg2 made more hydrogen than the replicate, but potentially it could have made even more hydrogen if dewatering had been nominal.

RhRuHg13 was batched identically to RhRuHg6, except that RhRuHg6 used red HgO while RhRuHg13 used the finer yellow HgO. The differences in the two hydrogen curves over the initial portions of the SRAT cycle appear to be within the limits of data reproducibility. During the last six hours of reflux, however, the hydrogen generation rate in RhRuHg6 fell to 35% of that in RhRuHg13. One hypothesis is that the finer yellow HgO was more readily reduced to elemental Hg due to its higher exposed surface area, and subsequently was more rapidly steam stripped from the slurry. Reduced slurry Hg concentrations allow the catalyst(s) to stay more active and make more hydrogen. The data for RhRuHg6 and RhRuHg13 suggest that this could have been occurring in the last half of the SRAT reflux period

There was one other difference between RhRuHg6 and RhRuHg13. RhRuHg6 received 20 mL of formic acid in a rapid burst at the very beginning of formic acid addition. The run was paused to confirm this by weighing the formic acid tray head on the dispenser. The total formic acid volume target was dropped 20 mL to compensate for the premature addition, and formic acid feeding was resumed. All indications are that the correct amount of formic acid was ultimately added to the run. The time spent reweighing the formic acid tray, checking the math, and resetting the volume target effectively offset the potential processing time gained from adding 20 mL in a burst instead of over about 25 minutes. Nevertheless, there are two potential reasons why RhRuHg13 is more comparable to the majority of the matrix runs than RhRuHg6.

RhRuHg12 (low Hg) is fairly similar to RhRuHg6 and RhRuHg13 (high Hg) in terms of hydrogen generation rates for about the first two hours after formic acid (Rh controlled period). This low Hg run, however, always produced more hydrogen than the two high Hg runs during the SRAT. The effect of initial Hg concentration is most obvious from +2 to +8 hours after formic acid. RhRuHg13 appears to be catching up to the RhRuHg12 generation rate near the end of the SRAT. RhRuHg12 and RhRuHg13 both used yellow HgO, but there was five times more in RhRuHg13 which must have taken longer to steam strip down to an ineffective concentration. RhRuHg6, starting with red HgO, did not appear to be catching up to the RhRuHg12 generation rates near the end of the SRAT.

The four sets of CO_2 data are given in Figure 12.

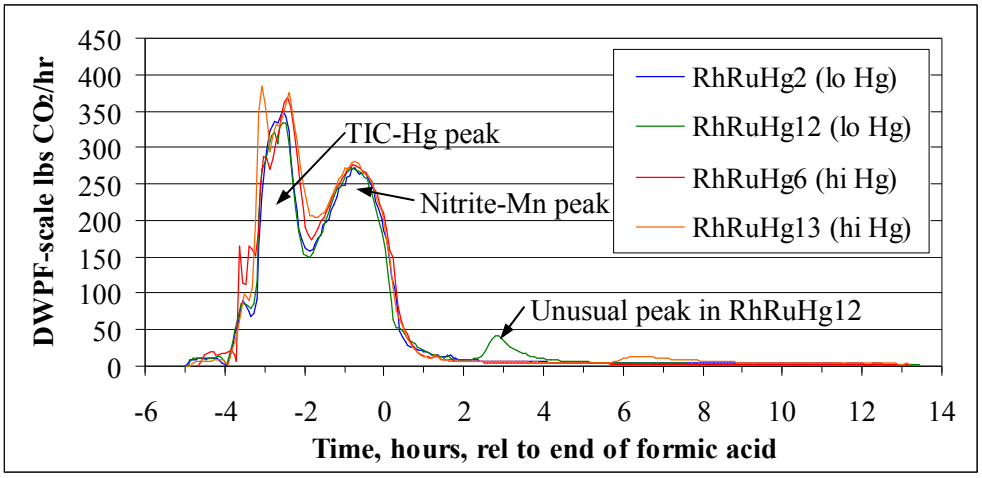

Figure 12. CO_2 at high Rh-low Ru

The four CO_2 peaks from nitrite-Mn reduction were well aligned confirming the acid additions were close to target. Some differences in magnitude were expected between -2 and -4 hours due to the two different initial concentrations of Hg. RhRuHg12 had an unusual peak at about +3 hours after formic acid addition that was unique in the matrix study. It should be indicative of heightened catalytic activity. The cause is unknown, but it was not replicated in RhRuHg2 perhaps due to the other issues with that run. The two low Hg runs produced 49.0 and 49.6 g of CO_2, while the two high Hg runs produced 52.8 and 55.7 g of CO_2, or an average increase of 4.95 g that was 2.0 g above the anticipated gain of 2.95 g due to the increased Hg alone. This extra CO_2 is mentioned because the difference was between two averages of pairs of runs rather than between two single runs, so some of the normal data reproducibility issues could have been mitigated by averaging. The difference could reflect a change in nitrite destruction chemistry.

Corresponding data for N_2O are shown in Figure 13.

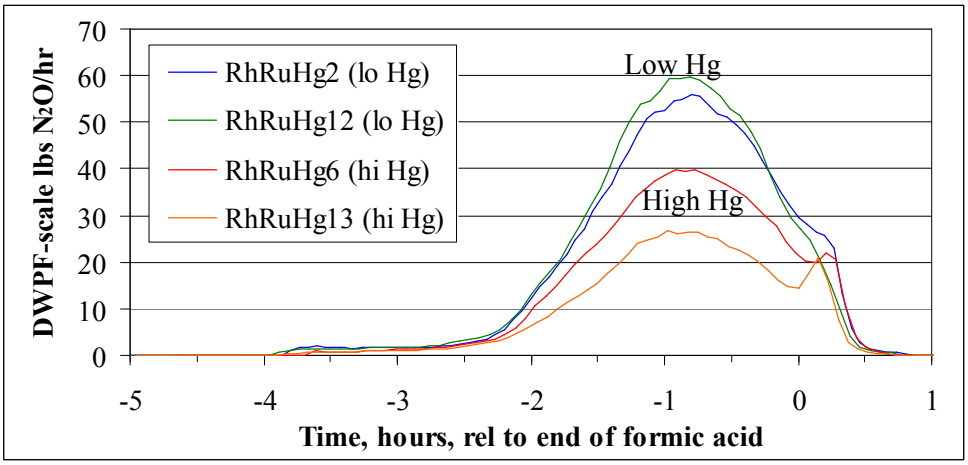

Figure 13. N_2O at high Rh-low Ru

The combination of high Rh with low Ru and low Hg produced the maximum N_2O generation rates for the entire twelve run matrix, 55-60 lbs/hr. The other ten peaks were below 45 lbs/hr. In the bead-frit tests with the matrix simulant, the case with no Hg and no noble metals peaked at 91 lbs N_2O/hr or about 30-40 lbs/hr more than the low Hg cases in the Rh-Ru-Hg matrix. RhRuHg6 was the only high Hg run that exceeded the N_2O production of the matrix midpoint. These data were consistent with recent findings indicating that Rh is a catalyst for N_2O production. The two high Hg runs made less N_2O than the two low Hg runs. The combination of high Rh with low Ru and high Hg in RhRuHg6 produced the maximum N_2O generation rates for the high Hg runs (above the midpoint levels). Production of N_2O seemed to be somewhat inhibited in the replicate, RhRuHg13 (a 30% drop which is hard to attribute to reproducibility in the case of N_2O data). RhRuHg13 peaked below the matrix midpoint in N_2O generation rate.

More initial mercury correlated with reduced N_2O formation. The mechanism is not understood. This trend was similar to both the low Rh-low Ru and low Rh-high Ru cases and to SB4 runs.[12] The SB3 impact of Hg on hydrogen study results at three levels of Hg were more ambiguous except that the data indicated that no Hg gave the most N_2O compared to 0.11 and 2.0 wt% Hg in the initial sludge total solids.[5] The effect of shaft corrosion was not particularly evident in the N_2O data for the RhRuHg2-RhRuHg12 pair; however the shaft was just beginning to corrode during the period of N_2O generation.

3.1.5 High Rh-High Ru Results

The impact of two levels of mercury on the hydrogen generation rate profiles at 0.0133% Rh and 0.050% Ru (maximum Rh and Ru case) is shown in Figure 14. The RhRuHg8 GC drifted 9.2% in calibration during the SRAT cycle. The two runs used different He mass flow controllers.

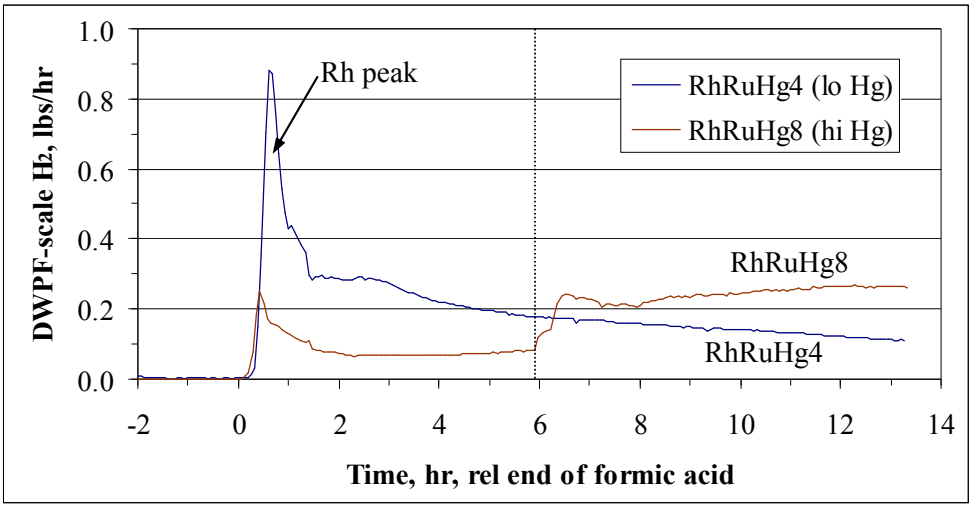

Figure 14. Hydrogen at high Rh-high Ru

The high Rh-high Ru-low Hg case produced the maximum hydrogen generation rate in the twelve run matrix. This was the anticipated result for maximum noble metal concentrations with the minimum mercury concentration. RhRuHg4 hydrogen results were probably enhanced by the corroding agitator shaft in much the same manner as those for RhRuHg2. This run must be

repeated to reduce potential artificial variability in the various potential measures of hydrogen production that are to be studied using statistical tools, since causes of variation are supposed to be limited to Rh, Ru, and Hg. RhRuHg8 had a maximum hydrogen generation rate about 50% higher than the next closest three tests with high mercury. The peak rate was nearly a factor of ten higher than in the low Rh-low Ru-high Hg run. Variation among the runs with low Hg was not as pronounced.

The high Hg test hydrogen generation rates passed those in the low Hg test at high Rh-high Ru about six hours after the end of formic acid addition. This reversal was unexpected. A number of instances were noted where changes in relative chemistry occurred about six hours after formic acid addition, and these may be related to the time that Hg was effectively removed from the SRAT in terms of its inhibiting power. However, the low Rh-low Ru runs exhibited similar hydrogen generation rate change behavior. That changeover came in the SME, instead of in the SRAT, but may have occurred for similar reasons related to the interactions occurring between mercury and the noble metals (probably Ru).

The CO_2 data for RhRuHg4 and RhRuHg8 are given in Figure 15.

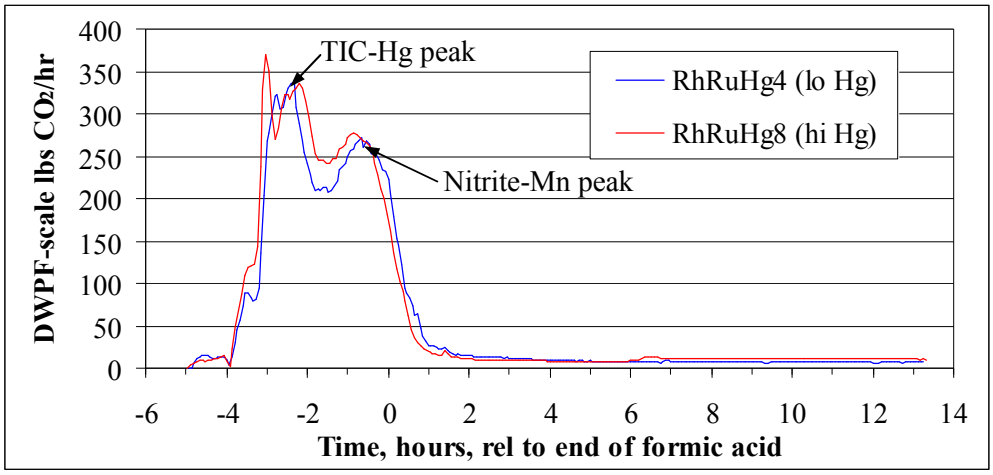

Figure 15. CO_2 at high Rh-high Ru

The RhRuHg8 nitrite-Mn reduction peak seemed to end slightly sooner than the RhRuHg4 peak (largest visible timing difference of any pair of about ten minutes) which might indicate a small (2-4%) difference in total acid in some SRAT simulations, but no significant difference was noted in the before and after weights of the acid trays relative to the targets. Significant catalysis of nitrite destruction by Hg and/or the noble metals may have been occurring in RhRuHg8, bringing nitrite destruction to an earlier end. Hg may itself be a catalyst for nitrite destruction, or it may be promoting one of the other noble metals acting as the catalyst, causing more rapid formation of NO from formic acid reduction of nitrite ion. Strong supporting evidence for some sort of enhanced nitrite to NO destruction effect was obtained in the bead-frit 4-L matching test that included 1.5 wt% initial Hg with 0.2 wt% Ru. Additional solid data for Rh catalyzed nitrite destruction were also obtained from the 22-L tests.[13] RhRuHg8 produced 59.8 g of CO_2 overall versus 55.5 g in RhRuHg4, or 4.3 g more overall compared to 2.95 g expected from the

increased Hg alone. The remaining 1.35 g difference or 3% lies within the reproducibility of the data.

The N_2O data for this pair of runs are shown in Figure 16.

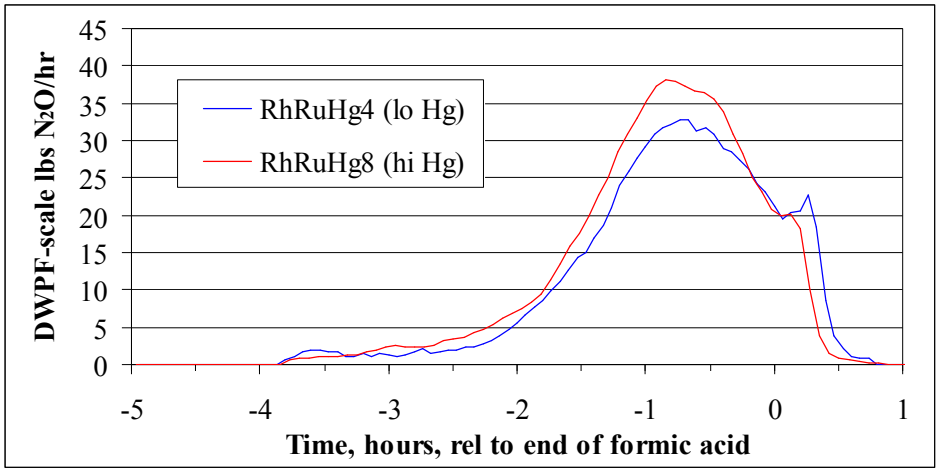

Figure 16. N_2O at high Rh-high Ru

This pair of N_2O generation curves showed the high Hg case producing more than the low Hg case, which reversed the trend of the other three Rh-Ru cases and was closer to what was seen in the SB3 impact of Hg study (that a clear trend was hard to discern for cases with nonzero Hg).[5] Rh is a catalyst for N_2O formation, and it was at the maximum concentration here. RhRuHg8 only made 10% more total N_2O overall than RhRuHg4, 3.25 g versus 2.93 g, so the difference may lie within the range of reproducibility of N_2O data.

RhRuHg4 had one of the clad agitator shafts that corroded badly which could have produced potential bias in some of the data. The low Hg run completed N_2O generation later than the high Hg run, consistent with the CO_2 data, which were slightly offset as well and in the same direction. This pair was the only pair in the test matrix to show a clearly visible offset in event timing near the end of acid addition. While this could have been due to an undetected delta in total acid, it more likely indicates that the high Rh-high Ru-high Hg run was the most reactive of the nine systems for nitrite destruction and succeeded in destroying it the fastest.

3.2 Other Comparisons of H_2 Data

Hydrogen data were given above in pairs of low-high Hg values at constant Rh-Ru values, but several other graphical comparisons are possible and informative. Figure 17 compares the hydrogen generation rate profiles for the runs with the smallest Rh concentration covering the four possible Ru-Hg combinations. The legends in this section show Rh-Ru-Hg in that sequence with L=low and H=high, rather than run ID numbers.

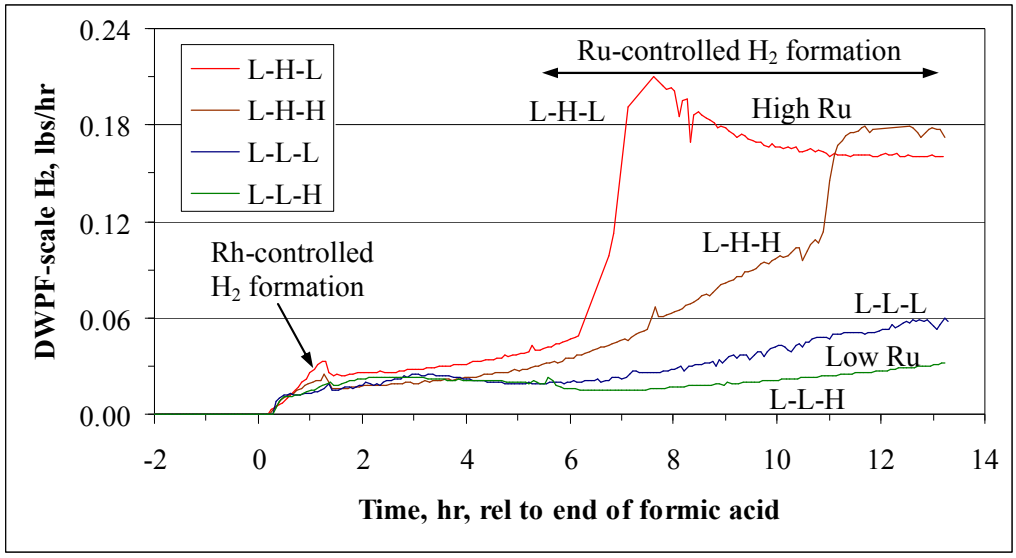

Figure 17. Comparison of all low-Rh H_2 data

The profiles from 0-3 hours after the end of formic acid are all nearly identical suggesting that Ru and Hg did not have a big impact on early hydrogen generation rates (mercury may have been a weak inhibitor of Rh). The high Ru pair had slightly higher peak generation rates in the first two hours after acid addition than the low Ru pair, but these differences are only about 10-25%, i.e. within the expected accuracy of the measurements to discriminate differences of ~10%, but near the limit of historical reproducibility for 4-L runs of about 25-30%. Adding other noble metals to Rh in the bead-frit work led to reduced peak generation rates, but those tests had no mercury and order of magnitude greater noble metal concentrations.[9]

The two runs with low Rh-high Ru appeared to have an activation time for increased hydrogen generation. The L-H-L run surged at about +7 hours and the L-H-H run surged at about +11 hours. Both occurred in the period that preliminary statistical modeling shows is dominated by Ru catalysis. The delay in the run with higher Hg may be an effect of the Hg itself. Preliminary statistical modeling has not linked Ru and Hg together during this period, but that may be due to the way the graphical data was reduced to simple numerical measures. Previous researchers who have reported on an induction period for noble metal catalyzed decomposition of formic acid have found that Ru takes longer to become active than Rh or Pd.[14]

Three of the four runs, L-L-L, L-H-H, and L-L-H, used the same He mass flow controller. Maximum GC calibration drift was 3% in this block of four runs. Consequently, measurement precision was fairly well controlled in this block, so differences are expected to be real within the reproducibility limits (which may drop into the 10-20% range with the measurement precision here).

Figure 18 gives all of the high Rh data (six runs) on a single plot. There are six sets of data covering the four Ru-Hg combinations plus two replicate trials.

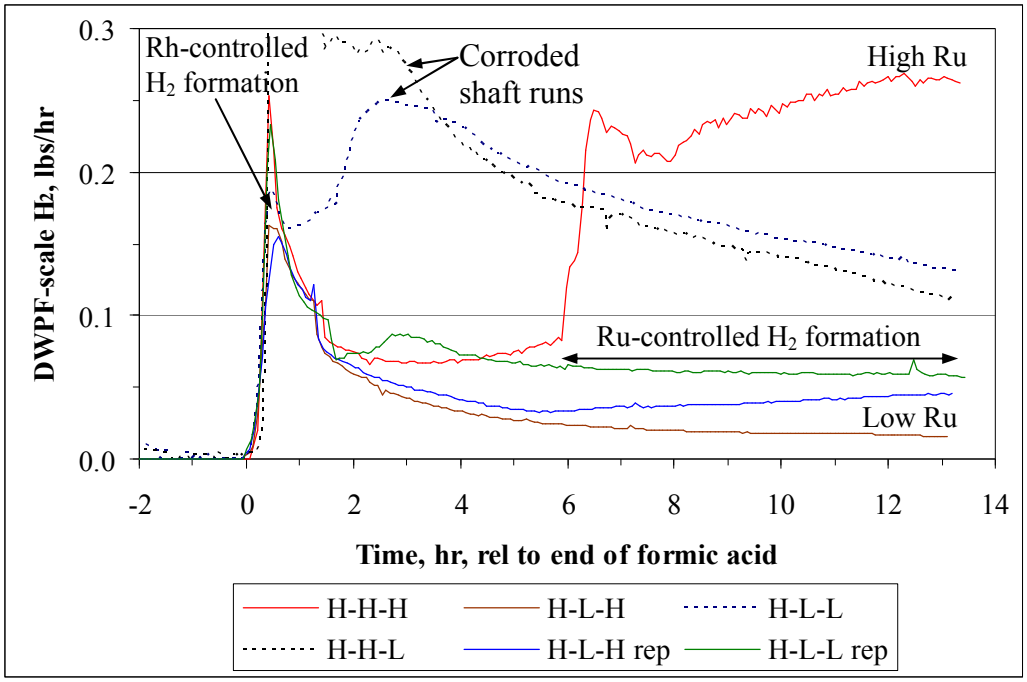

Figure 18. Comparison of all high-Rh H_2 data

Data from the two runs with corroded shafts are shown as dashed curves based on the earlier discussion. Both runs seem to be out of place with respect to the balance of the data for high Rh runs. Both runs should be rejected from inclusion into the final matrix database used for statistical evaluations. That leaves the Rh-Ru-Hg matrix unbalanced (only 7/8th complete), short a replicate, and potentially unable to distinguish between a main effect and a two-way interaction effect that were strongly correlated.

The four other high Rh runs behaved fairly similarly during the period from near the end of formic acid addition until several hours later. Statistically significant variations existed in the peak height during this period generally trending such that more Hg led to lower peak rates. The single uncorrupted high Ru run (H-H-H or RhRuHg8) made significantly more hydrogen later in the reflux period than any of the three low Ru runs. This indicated a strong impact of Ru toward the end of the SRAT. The two runs H-H-H and H-L-H rep used the same He mass flow controller. The other four runs used four different He mass flow controllers. The H-H-H run drifted 9.2% in hydrogen calibration during the SRAT. The other five runs stayed within 4% of calibration for hydrogen.

Data from the four high Ru runs are collected in Figure 19. There are four sets of data covering the four Rh-Hg combinations at high Ru.

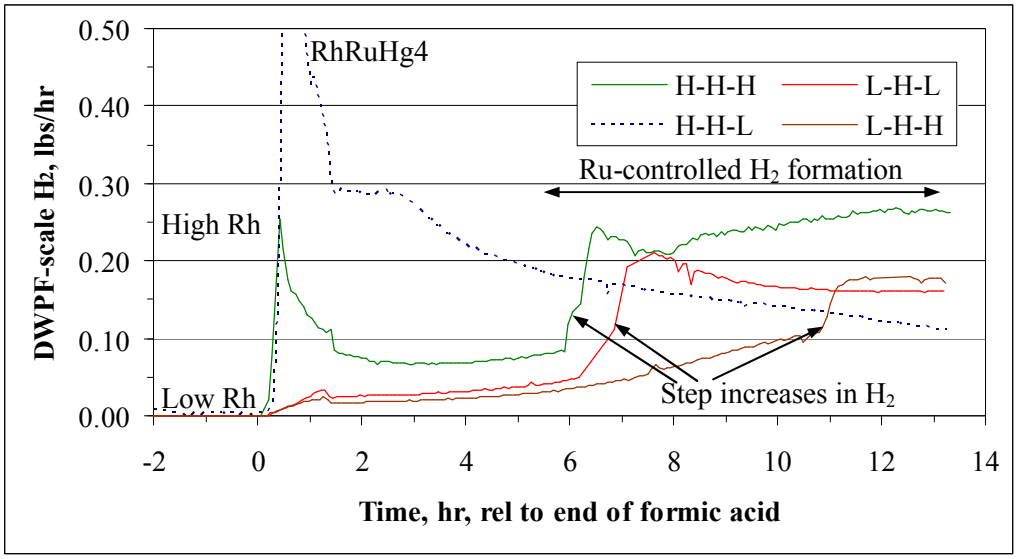

Figure 19. Comparison of all high Ru H_2 data

Ru is a constant on this graph. The variations seen must be due to one of the other two factors or an interaction. The data from RhRuHg4 (H-H-L) with the corroding shaft seem fundamentally different from the data for the other three runs. The other three runs have a step increase in H_2 generation in the middle to late stages of reflux that is absent in RhRuHg4. This difference seems to support the need for repeating RhRuHg4 and replacing its data in the matrix. Identifying the cause for the step increase in hydrogen generation during the middle of reflux in the other three runs may merit further investigation. The step change occurred sooner in the high Rh-high Hg and low Rh-low Hg cases, i.e. the two extreme Rh-Hg pairs, than in a mixed high-low case. This suggests that the cause may lie partially outside of the three factors in the matrix study. These four runs all had different He mass flow controllers.

Finally, the low Ru data are presented in the same manner as the high and low Rh and high Ru data in Figure 20. There are six sets of data covering four Rh-Hg combinations. Only one of the six data sets is related to a run with a corroded shaft.

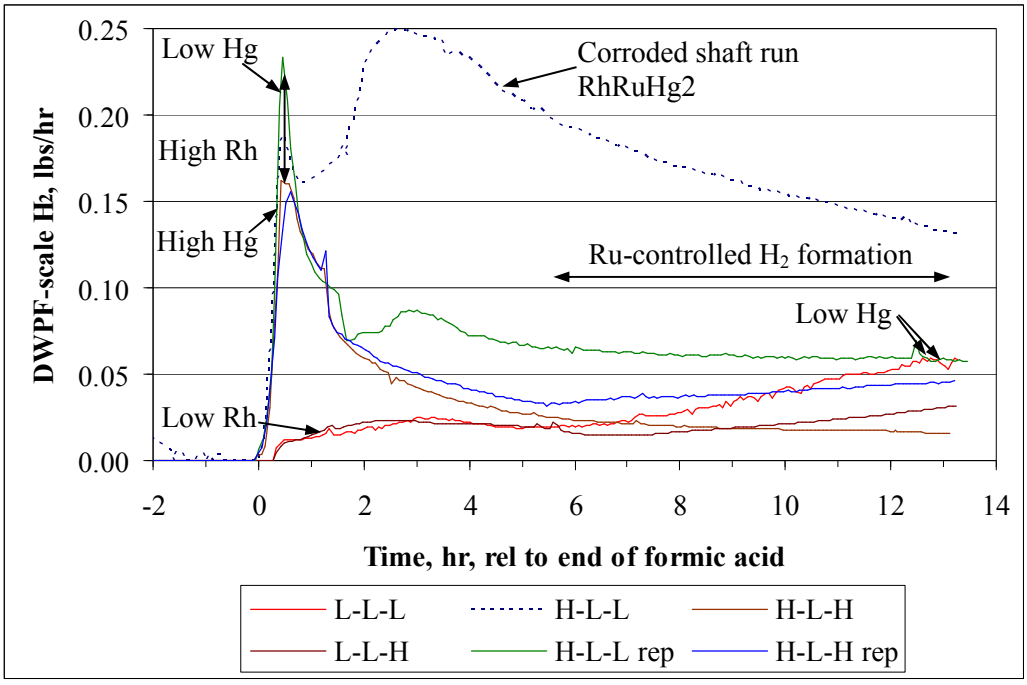

Figure 20. Comparison of all low Ru H_2 data

RhRuHg2 (H-L-L) data are not similar to any of the other five runs starting one hour after the end of formic acid addition. It seems likely that this is due to the shaft corrosion issue rather than normal random variations in data reproducibility. The five other runs became fairly similar during reflux. The difference between high and low Rh is obvious in the 0-2 hours after acid period. The high-low mercury impact at high Rh is also fairly obvious in this time frame. The low Ru data lack the step changes seen in the high Ru data, Figure 19. The runs L-L-L, L-L-H, and H-L-L all used the same He mass flow controller and had less than 3% drift in hydrogen calibration. The other three runs used three different He mass flow controllers and had less than 4% drift in hydrogen calibration.

The last two figures both show considerably more H_2 generation in the two corroded shaft runs relative to the other runs in the period from 2-6 hours after the end of acid. This H_2 generation is likely a by-product of the corrosion reaction itself (acid oxidation of elemental metals), since negligible additional CO_2 was formed. Catalytic destruction of formic acid is expected to produce both H_2 and CO_2 simultaneously.

The bead-frit data with this simulant showed that both Ru and Rh are active for hydrogen generation during the SRAT cycle, but that Rh can drive a large peak generation rate near the end of nitrite destruction. Conversely, Ru was observed to activate after nearly complete nitrite destruction. That is, Ru activated after the period of maximum Rh activity. The early Rh peak has the potential to be the maximum SRAT hydrogen generation rate.[9] The data in the Rh-Ru-Hg matrix study are consistent with this picture. The addition of Hg into the testing, however, had the largest impact on the initial hydrogen peak associated with Rh. As the initial Hg concentration increased, the initial Rh-driven maximum in the hydrogen generation rate

decreased. Hg may be accomplishing this by promoting nitrite destruction, and consequently shortening the life cycle of a nitro-Rh complex catalyst. The introduction of Hg created scenarios where the initial Rh-driven peak H_2 generation rate was not the largest H_2 generation rate during the SRAT cycle. The high Hg tests in the matrix study often had the maximum hydrogen generation rate occur after the initial Rh-driven period. As the ratio of Hg/Rh increased, the peak rate tended to occur later.

The range of Hg starting concentrations used in the matrix study, however, did not seem to be able to change the timing of the initial climb in hydrogen generation rates. With constant Rh, the H_2 generation rate began to climb nearly simultaneously. At most there are only small shifts in timing in the data. Such shifts would be expected if nitrite destruction was controlling both the activation and deactivation of the Rh catalyst during this part of the SRAT cycle, and if Hg was changing the rate of nitrite destruction.

The four high Ru tests produced about 0.21 lbs H_2/hr (0.16-0.26) at the end of reflux, while the six low Ru tests produced about 0.04 lbs H_2/hr (0.016-0.058). These rates are roughly in the ratio of 5:1 just like the nominal matrix ratio of high Ru to low Ru. It would be reasonable to expect that hydrogen generation rates in the last four hours of reflux were statistically correlated with the Ru concentration. Preliminary statistical modeling confirms this. There did seem to be a smaller trend for the low Hg runs to outperform the high Hg runs during the last four hours of reflux in the sets of constant Ru concentration. The bead-frit matching test with 0.2 wt% Ru and 1.5 wt% initial Hg had a very similar hydrogen generation rate profile to the two bead-frit tests with 0.2 wt% Ru and no Hg.[9] These data are not inconsistent with a weak Hg effect in the matrix data, since the initial Hg/Ru ratios were centered about 50 in the matrix study compared to 7.5 in the bead-frit matching test. The matrix study would tend to magnify any effect of Hg relative to the earlier bead-frit matching test because of the relatively higher Hg/Ru ratios. Nonetheless, changing from 0.5 to 2.5 wt% initial Hg had only a mild impact on the Ru-driven hydrogen generation rates. This lack of inhibiting potency could be related to the efficiency of Hg removal by steam stripping prior to the period of Ru-dominated hydrogen generation, or it could simply indicate that the effect of Hg on Ru catalysis is weak.

One hypothesis was advanced for the impact of Hg on hydrogen generation that involved the formation of an amalgam between one or more of the noble metals with liquid elemental Hg. Subsequent steam stripping of the Hg could leave behind a spongy, open structure of the noble metal that could exhibit enhanced activity. This sequence could either suppress or enhance the early activity of the catalyst (depending on the relative activity of the noble metal in the amalgam versus not in the amalgam) as the Hg concentration increases, but the subsequent activity of the noble metal catalyst would be expected to be enhanced if the initial Hg concentration was high.

Data supporting the mercury amalgam hypothesis were not obvious in the matrix study. Generally, low Hg runs had a slight advantage over high Hg runs in the latter stages of the SRAT when Hg has been significantly removed rather than vice versa. Four of the five high Hg runs had hydrogen generation rates trending upwards while only one of the five low Hg runs was trending upwards (corroding shaft runs excluded from consideration). It could be argued that a more active Ru catalyst was forming as the Hg was being steam stripped, but this doesn't prove the existence of Hg-Ru amalgams. Data on this sludge system were obtained by X-ray

absorption spectroscopy for sludge with Ru and for sludge with Ru plus Hg using samples taken before and during hydrogen generation.[15] It appeared that the Ru was primarily in the +4 oxidation state during both SRAT cycles rather than in the elemental state. This evidence indicates that there probably was no significant elemental Ru or Hg-Ru amalgam in the slurry.

3.3 SME Data Discussion

Six sets of SME cycle hydrogen generation data were obtained on the high-high, low-low, and midpoint-midpoint Rh-Ru runs. These six runs all had prototypical Rh/Ru ratios matched to the expected relative fission yield of 1/3.75. SME cycles were performed to expand the database of SRAT/SME runs with hydrogen. Factors relating the SME cycle hydrogen generation rates to the SRAT cycle hydrogen generation rates are under investigation. No statistical matrix study was performed on the SME cycle, since no suitable basis for such a study has been identified. The six new runs provide five new combinations of Rh-Ru-Hg plus one replicate to the available database. Each SME cycle had two canister decon water additions and dewaterings followed by two frit slurry additions and dewaterings. The three dips in the six SME off-gas profiles are between the four additions. Gas generation rates fall as heat is removed and the SME is cooled by the addition of room temperature water and frit slurry. Dilution also occurs with each addition, which generally tends to reduce kinetic reaction rates. Dewatering concentrates the slurry, causing reaction rates to rise (everything else being equal or constant).

3.3.1 Low Rh-Low Ru SME Data

Graphs were created for the SME cycle off-gas data with a zero set about 20 minutes prior to the start of the first decon canister dewatering. Data from the last two hours of reflux in the SRAT cycle are shown in the period from -3 to -1 hours to permit repeatable visual comparisons of the SME hydrogen or CO_2 generation rates to the corresponding SRAT rates. Data for the low Rh-low Ru runs are shown in Figure 21.

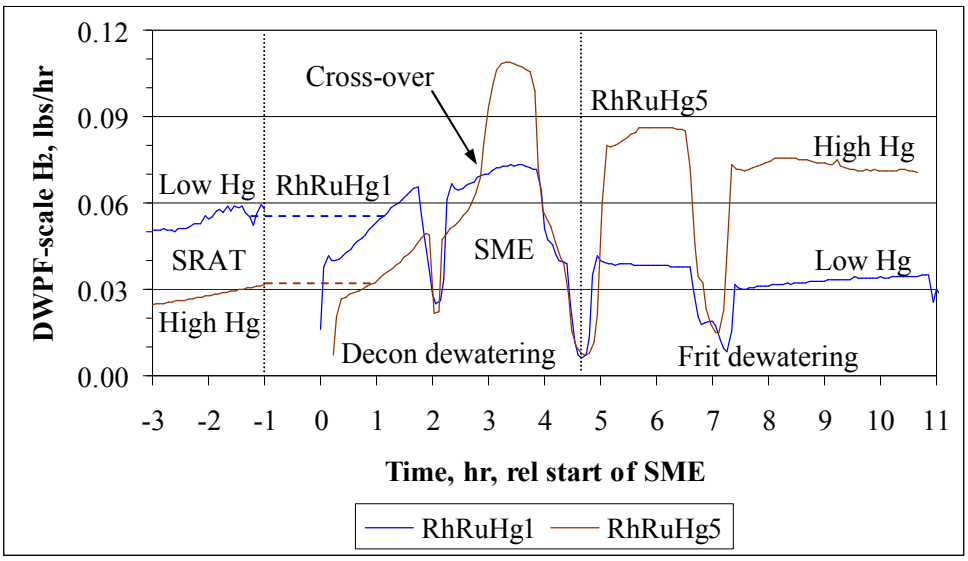

Figure 21. SRAT-SME Hydrogen at low Rh-low Ru

The high Hg run, RhRuHg5, passed the low Hg run in terms of hydrogen generation rate during the second canister dewatering of the SME cycle (arrow). The initial SME hydrogen generation rates were very similar to the end of SRAT reflux hydrogen generation rates (dashed connecting lines). This graph reemphasizes the point that initial conditions that bound the SRAT hydrogen generation rates, e.g. lower initial Hg in this comparison, do not necessarily imply that those conditions will automatically bound the SME cycle hydrogen generation rates. (It has been observed in numerous instances that the maximum hydrogen generation rate in the SRAT does not necessarily bound the maximum hydrogen generation rate in the SME. The lack of correlation between the two maximum rates was reported on previously.[10]) Sludge batch qualification testing in the SRNL Shielded Cells is the only way to validate a proposed acid addition strategy for a new sludge batch at this time.

The pattern for CO_2 followed that of hydrogen, Figure 22.

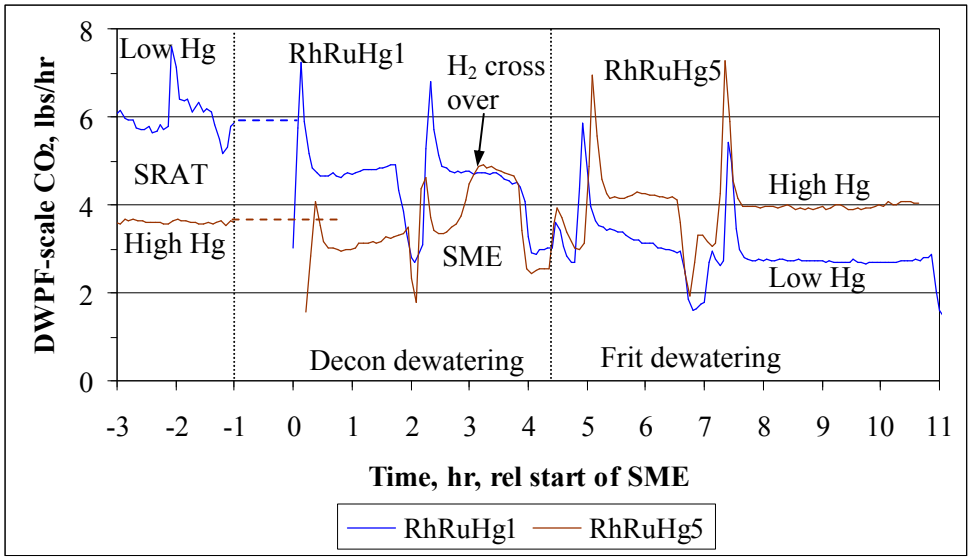

Figure 22. SRAT-SME CO_2 at low Rh-low Ru

CO_2 production in RhRuHg5 caught up to the production of RhRuHg1 simultaneously with the hydrogen cross over in Figure 21 (arrow). The data are not accurate enough to conclude that RhRuHg5 CO_2 production actually passed RhRuHg1 at this time; however, it was clear that RhRuHg5 was producing more CO_2 than RhRuHg1 a few hours later. Total SRAT CO_2 mass and percent formate loss were very comparable between this pair of runs, so it is not clear what process was driving the increase in RhRuHg5 catalytic activity relative to RhRuHg1 during the SME cycle unless a more active catalyst phase had formed in RhRuHg5.

3.3.2 Midpoint Rh-Midpoint Ru SME Data

Two SRAT-SME runs were performed at the midpoint noble metal and mercury concentrations of the Rh-Ru-Hg matrix, RhRuHg9 and RhRuHg11. Hydrogen generation rate results from the end of the SRAT cycle and during the SME cycle are shown in Figure 23.

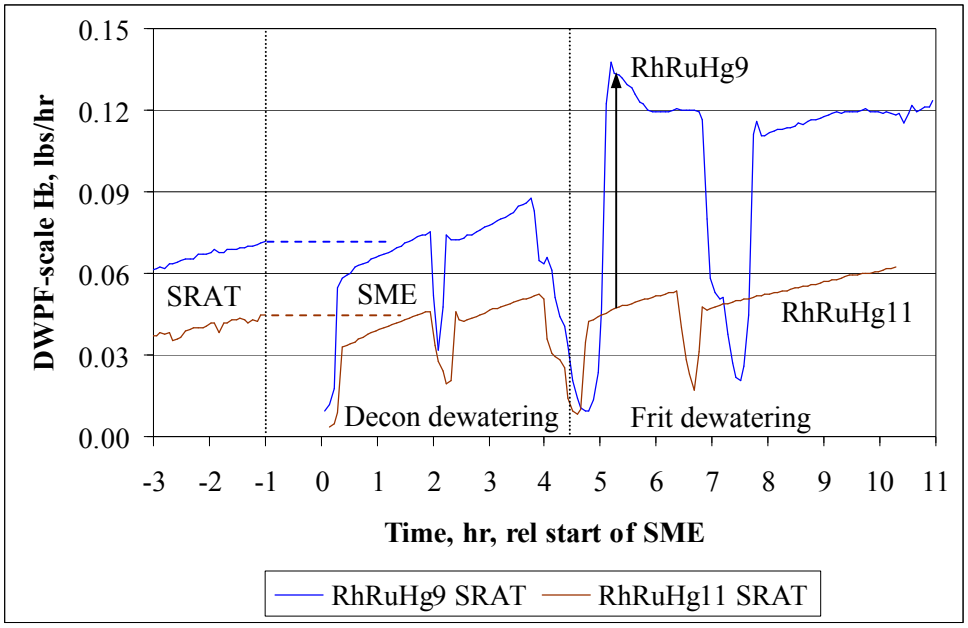

Figure 23. SRAT-SME hydrogen at midpoint conditions

There was no expected impact of Hg on these data, since both midpoint runs used identical Hg loadings. RhRuHg11 produced about 60% as much hydrogen as RhRuHg9. This difference was generally similar to the SRAT difference between this pair of replicate runs. The transition from the SRAT to the SME occurred with fairly consistent H_2 generation rates. The addition of formic acid with the first SME frit addition had a much more significant impact on RhRuHg9 than on RhRuHg11 (arrow). Corresponding CO_2 data are given in Figure 24.

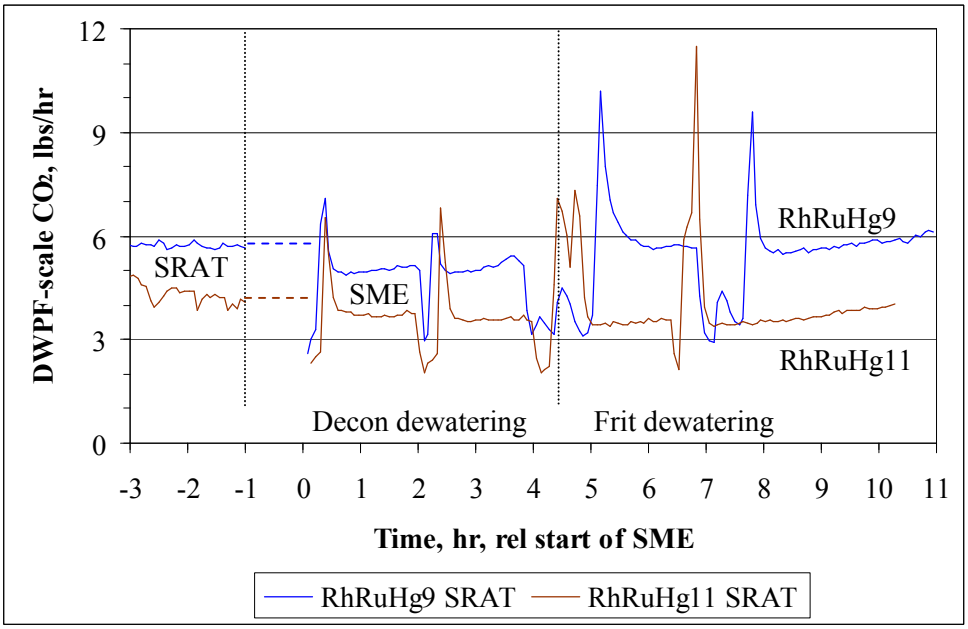

Figure 24. SRAT-SME CO_2 at midpoint conditions

The CO_2 data were very similar to the H_2 data in appearance, although the relative gap was somewhat smaller than for H_2 at the start of the SME. The transition from SRAT to SME occurred with minimal change in the catalytic CO_2 generation rate. The frit formic acid only produced a sustained increase in CO_2 generation rate for RhRuHg9 similar to what was seen with hydrogen. After the first frit formic acid addition, both the RhRuHg9 H_2 and CO_2 production rates were about double those in RhRuHg11. The processing differences within this pair cannot be attributed to any obvious factor, since both runs targeted identical conditions.

3.3.3 High Rh-High Ru SME Data

Two SME cycles were completed with the high Rh-high Ru combination, one at low Hg and one at high Hg. These were runs RhRuHg4 and RhRuHg8 respectively. The hydrogen generation rate data from the end of the SRAT and for the SME cycle are shown in Figure 25.

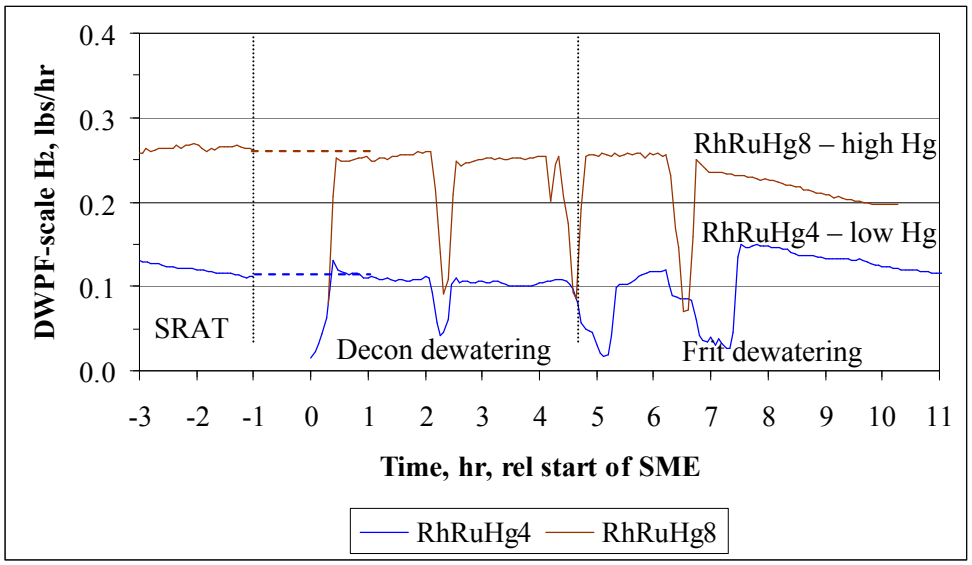

Figure 25. SRAT-SME hydrogen at high Rh-high Ru

There was good agreement between the end of SRAT and initial SME cycle hydrogen generation rates for the two cases. The hydrogen generation rates for the high Hg case were greater than those for the low Hg case throughout this period. RhRuHg8 actually exceeded the DWPF SME limit of 0.223 lbs hydrogen/hr. Both SRAT formate loss and total CO_2 production were also greater in the high Hg case than the low Hg case. These two results support the conclusion that the high Hg run was more catalytically active than the low Hg run. This was also the case eventually in the low Rh-low Ru SME cycle. Therefore, Hg can apparently act as a promoter for catalytic hydrogen generation under certain conditions, instead of as an inhibitor. The role of promoter could be through a process that forms a more catalytically active noble metal phase as the noble metal solidifies from an amalgam with Hg, though conclusive evidence for the presence of elemental noble metals is unavailable. Mercury had appeared to be an inhibitor for some of the Rh-catalyzed peaks shortly after acid addition, including the runs in this study.

The associated CO_2 data for this pair of runs are given in Figure 26.

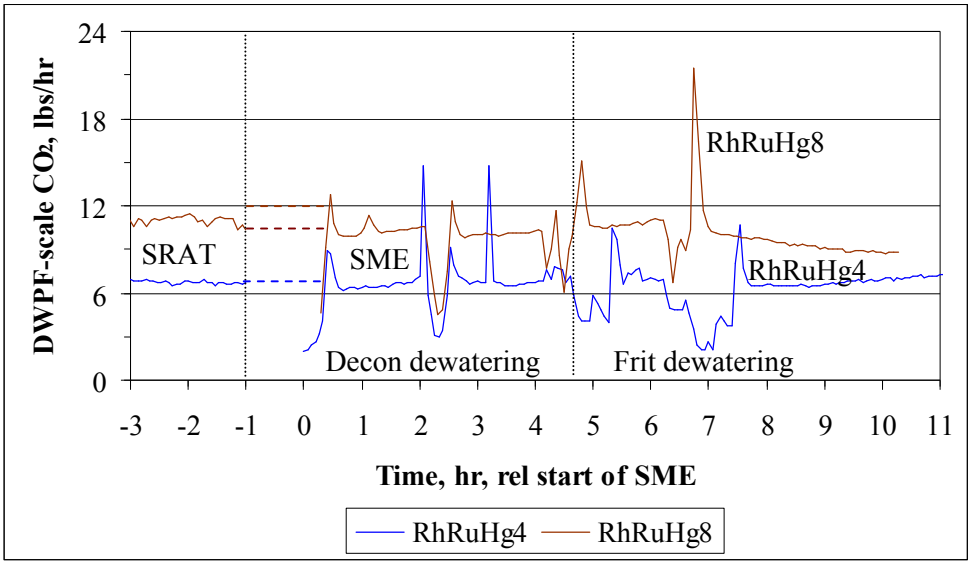

Figure 26. SRAT-SME CO_2 at high Rh-high Ru

The CO_2 data followed the same general trends as the hydrogen data. There was more formate conversion to CO_2 in the high Hg run than in the low Hg run. The two pairs of frit formic acid additions had very little impact on either the H_2 or CO_2 generation rates once boiling was resumed. It was expected that these additions would lead to increased H_2 and CO_2 production relative to the canister decon dewaterings that preceded them based on data from previous SME cycles.

3.3.4 SME summary

Several observations were made on the SME cycles. Generally the hydrogen generation rates during the first canister decon dewatering period were comparable to those at the end of the SRAT cycle reflux period. The implication is that the cool down and heat-up between SRAT and SME along with the ~15% dilution from the canister water were not having a major impact on the hydrogen generation rates under the conditions of the matrix tests. Ignoring the momentary surges in measured hydrogen generation rate that immediately followed boiling and included the liberation of accumulated H_2 in the vessel, the initial SME H_2 generation rates near the start of the first canister dewatering tended to be slightly less than those at the end of the SRAT. This decrease is consistent with a kinetic mechanism containing one or more concentration dependences to a positive power combined with the diluting effect of the canister water addition on those concentrations. These observations were also applicable to the CO_2 generation rate behavior.

The impacts of the formic acid-frit slurry additions on the hydrogen generation rates seemed fairly muted compared with some of the historical data that show significant step increases in hydrogen generation following each frit addition. These increases were always attributed to the increase in formate concentration, or the drop in pH, or the combination of both. Some of the

formic acid-frit slurry additions in the matrix study qualitatively resembled canister decon water additions, or perhaps frit slurry additions without formic acid. Assuming the formic acid was added as planned, however, it would be reasonable to propose that neither formate ion concentration nor pH were controlling the H_2 and CO_2 generation rates at this point in the process during some of the Rh-Ru-Hg matrix runs.

The two pairs of SME cycles were completed from pairs of SRAT cycles having a high and low initial Hg concentration. The runs with the higher Hg concentration finished with higher hydrogen and CO_2 generation rates than the corresponding low Hg runs both times. This is the opposite of the expected impact of Hg on hydrogen generation and catalytic activity. It may be due to the extent of mercury removal that has occurred during the SRAT, and the effect of this on the form of the active catalyst species during the SME. Apparently, the initial concentration of Hg is an important factor impacting both SRAT and SME hydrogen generation rates. Therefore, continued emphasis on the accurate determination of the mercury content of new sludge batches is strongly recommended prior to simulant pre-qualification testing.

This page intentionally left blank.

4.0 CONCLUSIONS

Simulations of the DWPF CPC vessels were performed as part of the ongoing investigation into catalytic hydrogen generation. Rhodium, ruthenium, and mercury have been identified as the principal elemental factors affecting the peak hydrogen generation rate in the DWPF SRAT for a given acid addition. The primary goal was to identify any significant interactions between the three factors. Noble metal concentrations were similar to recent sludge batches. Rh ranged from 0.0026-0.013 wt% and Ru ranged from 0.010-0.050 wt% in the dried sludge solids, while initial Hg ranged from 0.5-2.5 wt%.

A statistically-designed, experimental matrix was required to ensure that the existence of significant two-way interactions could be determined without confounding of the main effects with the two-way interaction effects. The test matrix was composed of twelve SRAT cycles. Testing included: a three factor study at two levels per factor (eight runs), two duplicate midpoint runs, and two additional replicates to assess reproducibility. The midpoint tests allowed for the identification of potential higher order (quadratic) effects from the three factors. Acid addition was constant except for small changes to offset changes in the starting mercury concentration. Six SME cycles were performed to supplement the SME hydrogen generation database.

Some of the findings from this study include:

- Preliminary data analysis indicates that additional SRAT runs are needed to replace suspect data in the original set of twelve runs prior to statistical analyses. These include another midpoint run and replacing both runs with corroding shafts.
- Corrosion chemistry during runs with the 400 series stainless steel shafts impacted the hydrogen generation rate.
- Rh was linked to the maximum SRAT hydrogen generation rate in the first two hours after acid addition.
- Ru was linked conclusively to the SRAT hydrogen generation rates in the last four hours of reflux.
- Decreasing the ratio of Rh/Hg shifted the noble metal controlling the maximum hydrogen generation rate from Rh to Ru in runs where Ru was at its fission yield ratio to Rh.
- The inhibiting effect of mercury on hydrogen generation apparently does not require much mercury in terms of moles Hg/mole Rh (or Ru), but once the initial impact is realized, the benefit of additional Hg in reducing hydrogen generation is minimal. Sludge Batch 3 and 4 simulant test data confirm this.
- Low Hg runs do not necessarily bound high Hg runs for hydrogen generation over the full SRAT-SME cycle. Two of the four Rh-Ru combinations had a cross-over point where the hydrogen generation rate in high Hg run went from always lower to always higher than in the low Hg run. One cross-over was in the SRAT and one was in the SME. The maximum hydrogen generation rate could occur in the high Hg run.
- SME cycle hydrogen was generated at rates similar to those at the end of the SRAT during the first decon canister dewatering period.

The additional SRAT runs are expected to refine the values in the final statistical matrix of run data so that the primary sources of error are due to the three factors, Rh, Ru, and Hg, and to the limits of reproducibility of the SRAT data. The runs will also help to evaluate whether or not the acid requirement of the sludge simulant changed over time. The pH 7 base equivalents will be rechecked as well for changes.

Enhanced hydrogen generation in the two runs with corroded shafts was unexpected. Hydrogen was apparently generated by the corrosion reactions themselves. Acid-driven corrosion reactions are known to produce hydrogen gas via oxidation of the metal element and reduction of the acidic proton. The only issue is whether or not the corrosion reaction(s) generated the majority of the additional hydrogen or whether there was a catalytic component.

The conclusions concerning the timing of the Rh and Ru catalyzed hydrogen generation reactions should extend to higher acid stoichiometries with equally rapid nitrite destruction. At lower acid stoichiometries, however, the destruction of nitrite is not nearly complete at the end of formic acid addition. A general rule has not been developed for this case. The delay in nitrite destruction simultaneously delays Rh catalyzed hydrogen generation. The interaction of the final stages of nitrite destruction in the SRAT, Rh deactivation and Ru activation occurring at the end of nitrite destruction, and the presence of fresh nitrite ion in the refluxed condensate following dewatering can give rise to a variety of hydrogen generation rate behaviors during reflux.

A more exacting analysis of the CO_2 data is planned in order to identify the timing of Hg reduction during acid addition. A fairly complete timeline of the major reactions occurring in the SRAT was developed from data with this simulant during the bead-frit test program. SME products from these runs, however, are to be processed through a pilot scale melter. Therefore these runs were performed without mercury in order to simplify melter off-gas concerns.

A more detailed statistical evaluation is expected to occur once the new replacement run data has been obtained. Once that has been completed, a summary of the current understanding of Rh and Ru catalyzed hydrogen generation in the DWPF CPC will be prepared that incorporates all of the new data obtained in the past year and a half.

5.0 RECOMMENDATIONS/PATH FORWARD

Five separate measures of SRAT hydrogen generation and seven measures of other SRAT chemistry were defined prior to performing preliminary statistical model evaluations. These showed variations in the outcomes of the modeling depending on which runs were included in the database. At least three additional SRAT runs are needed to address issues in the data before the originally planned statistical modeling and analysis can be brought to a satisfactory endpoint. These runs will address the corroding shaft issue and the shifting midpoint behavior issue, as well as ensuring sufficient replicates are available.

A study to evaluate deactivation of hydrogen generating reactions has been planned (was originally in the FY08 plan and was rescheduled for FY09). The need for this study should be reevaluated based on what has been learned. Rh appears to be activating and deactivating as nitrite destruction goes through its final stages. The activity of Rh after nitrite destruction appears to be significantly less than that of the more abundant Ru, although this has not yet been proven to be a universal result. Subsequently, there is some inferential evidence that Rh may be undergoing reduction by formic acid. Ru appears to be activating after nitrite destruction, and perhaps remains active throughout the rest of the SRAT and SME cycles. A slow process appears to be taking it out of solution and reducing its activity. The quantities of nitrite required to sustain a nitro-Rh complex catalyst are at or below normal IC detection limits for nitrite at the current Rh concentrations. Therefore, the nitrite-Rh complex chemistry would be difficult to study in a sludge simulant system, while studies in simpler systems might not apply to the SRAT.

By comparison, the task of understanding acid consumption in the SRAT does not appear to be as complex. Fairly simple analytical tests are able to distinguish which of the primary basic species in the sludge remain relatively inactive during the SRAT from those which give up their hydroxide or carbonate and consume acid. Considerable progress has been made in the past year on understanding nitrite destruction and Mn reduction. This information should be used to ensure that excess acid is not added to the SRAT by developing improved acid addition equations. Hydrogen generation can be controlled by limiting the quantity of excess acid added to the SRAT over the range of likely noble metal concentrations and wash endpoints that have been studied to date. This strategy can work as long as the SRAT processing goals can be met by an acid addition strategy that is safely removed from significant hydrogen generation, since uncertainties in the calculation of the acid requirement could still lead to an inadvertent addition of too much acid if the window between adequate and excessive acid is too small.

This page intentionally left blank.

6.0 REFERENCES

[1] Plodinec, M. J., *Report of the Hydrogen Generation Review Panel – Review of Hydrogen Generation in the DWPF*. March 15, 2007.

[2] HLW-DWPF-TTR-2007-0016, *Catalytic Hydrogen Generation Program*, B. A. Davis, March 8, 2007.

[3] Koopman, D. C., *Task Technical and Quality Assurance Plan – Catalytic Hydrogen Generation Program.* WSRC-RP-2007-00338, SRNL, Aiken, SC 29808 (April 2007).

[4] Koopman, D. C., *Analytical Study Plan for Catalytic Hydrogen Generation Program.* SRNL-PSE-2007-00154 (August 2007).

[5] Koopman, D. C. and M. A. Baich, *Effect of Mercury-Noble Metal Interactions on SRAT Processing of SB3 Simulants*. WSRC-TR-2004-00548, SRNL, Aiken, SC 29808 (December 2004).

[6] Koopman, D. C., *DWPF Hydrogen Generation Study – Form of Noble Metal SRAT Testing*. WSRC-TR-2005-00286, SRNL, Aiken, SC 29808 (July 2005).

[7] Koopman, D. C., *DWPF Hydrogen Generation Study: Phase II – Form of Noble Metal SRAT Testing*. WSRC-TR-2005-00420, SRNL, Aiken, SC 29808 (December 2005).

[8] Koopman, D. C., *Preparation, Characterization, and Preliminary SRAT/SME Testing of a Simulant for the Hydrogen and Rheology Modifiers Program.* SRNL-PSE-2007-00191 (September 2007).

[9] Koopman, D. C., *Noble Metal Chemistry and Hydrogen Generation during Simulated DWPF Melter Feed Preparation*. WSRC-STI-2008-00002, SRNL, Aiken, SC 29808 (May 2008).

[10] Koopman, D. C., T. B. Edwards, and M. D. Joner, *Summary of Findings Based on Statistical Analysis of a SRAT-SME Database*. SRNL-PSE-2007-00207 (October 2007).

[11] Baich, M. A., D. R. Best, M. E. Stone, and M. F. Williams, *Sludge Batch 2-3 Blend Flowsheet Simulations: Process Variability Study*, WSRC-TR-2004-00225, SRNL, Aiken, SC 29808 (May 2004).

[12] Baich, M. A., C. C. Herman, D. R. Best, M. F. Williams, and E. K. Hansen, *Sludge Batch 4 Initial Simulant Flowsheet Studies: Phase I SRAT Results*, WSRC-TR-2005-00194, SRNL, Aiken, SC 29808 (June 2005).

[13] Koopman, D. C., B. R. Pickenheim, and D. R. Best, *SRAT Chemistry and Acid Consumption during Simulated DWPF Melter Feed Preparation*, WSRC-STI-2008-00131, SRNL, Aiken, SC 29808 (July 2008).

[14] Müller, E. and W. Loerpabel, *The Catalytic Decomposition of Aqueous Solutions of Formic Acid by the Platinum Metals IV* (in German), Monatshefte für Chemie, **53**, 825 (1929).

[15] Fox, E. B. and B. R. Pickenheim, *Speciation of Ru and Hg during Simulated Nuclear Waste Processing*, SRNL-MST-2008-00151, SRNL, Aiken, SC 29808 (July 2008).

7.0 ACKNOWLEDGEMENTS

The author wishes to acknowledge the contributions of a number of people. One key element of this report was the noble metal sample data. Obtaining the samples during the process simulations added a considerable burden to the work load of the ACTL laboratory technicians. The efforts of J. W. DuVall, V. J. Williams, I. A. Reamer, R. J. (Phyllis) Workman, T. O. Burckhalter, and D. M. Marsh are especially appreciated in this regard. Various researchers assisted the technicians with data logging during the busier periods. Consequently thanks are also due to B. R. Pickenheim, M. E. Stone, E. B. Fox, and J. R. Abramczyk. Once the samples were pulled, they were mostly sent to Analytical Development. The high quality of the bulk of the ICP-MS data from L. C. Johnson was critical to developing some of the conclusions in this report, and his efforts were greatly appreciated. Additional analytical support was provided by the Process Science Analytical Lab, including D. R. Best, W. A. Thomas, and P. T. Simmons. Finally, a report on hydrogen requires gas composition data. Developing and validating the GC gas composition data was made more difficult by some anomalous behavior that developed in the instruments during processing. This was a relatively major issue during the eight frit runs. Thanks are due to J. M. Pareizs and M. F. Williams who maintained the GCs during the testing and reprocessed the GC data after the runs were over.

This page intentionally left blank.

APPENDIX A. ADDITIONAL SAMPLE RESULTS

This appendix presents some of the significant additional sample results from the twelve Rh-Ru-Hg matrix tests that were not documented in the main text. SRAT product slurry anions by IC, along with wt % total and insoluble solids for the SRAT products are summarized in Table 6.

Table 6. SRAT Product Anion and Solids Data

	Nitrate, mg/kg	Formate. mg/kg	Sulfate, mg/kg	Chloride, mg/kg	Wt % Total Solids	Wt % Insoluble Solids
RhRuHg1	30,300	61,900	n.a.	377	26.3	14.4
RhRuHg2	28,900	60,700	n.a.	377	26.3	14.5
RhRuHg10	28,400	62,900	n.a.	473	26.0	14.7
RhRuHg4	27,400	61,800	n.a.	477	26.7	14.8
RhRuHg5	31,200	62,800	n.a.	370	26.2	14.3
RhRuHg6	30,900	72,800	n.a.	374	26.0	14.4
RhRuHg7	29,200	61,400	n.a.	504	26.0	14.2
RhRuHg8	28,600	57,700	1360	522	26.0	14.2
RhRuHg9	26,500	61,200	n.a.	455	26.0	14.1
RhRuHg11	27,600	58,200	1440	419	26.1	14.4
RhRuHg12	28,800	59,100	1590	374	25.8	13.8
RhRuHg13	28,100	59,100	1570	375	26.1	14.3

Formate averaged lower in the last four tests (8, 11, 12, and 13) than in the first eight tests. The last four tests averaged 58,530 with standard deviation 695, while the seven early tests (neglecting RhRuHg6) averaged 61,810 with standard deviation 810. RhRuHg6 was 13 standard deviations off the initial group mean, i.e. an outlier. The distributions of the two groups do not overlap at two standard deviations from each mean (60,190 for the high seven versus 59,910 for the low four). This seems to indicate precision within samples analyzed together versus accuracy of the absolute numbers. The eleven similar values are within ±5% of 60,620 mg/kg which is better than the expected accuracy for formate measurements by IC of ±10%. The presence of a high average group and a low average group in this particular data set, however, has the potential to bias statistical analyses of factors affecting formate loss. One solution would be to reanalyze the SRAT product anions of the final runs in the statistical matrix over a one to two day period to achieve a data set with the precision of one of the two individual groups above.

Similar issues were seen with supernate sample results. Wt% total and insoluble solids were fairly consistent across the twelve runs. The SRAT target was 26.7 wt% total solids. Typical results are a little below target. Chloride generally tracked the amount of $RuCl_3$ trimmed into the run. Values of 370-377 ppm Cl were low Ru, values of 419-455 ppm Cl were midpoint Ru, and values of 473-522 ppm Cl were high Ru. An increase of about 135 ppm Cl was expected from low to high Ru.

Slurry samples were pulled thirty minutes prior to the end of the SRAT cycle and quenched with caustic to stop reactions. These samples were analyzed for anions to compare with the SRAT product anions (from unquenched SRAT product slurry samples), Table 7. These samples were taken in an attempt to reduce the uncertainty in the SRAT product anion results and to improve the statistical modeling of formate loss and nitrite-to-nitrate conversion. As discussed in the main body of the report, accurate modeling of the IC-based run data was difficult. Quenched sample analyses were not performed in duplicate for the first eight runs (1, 2, 4-7, 9, and 10), however, while SRAT product anions were always averages of duplicate measurements.

Table 7. SRAT Product Anions versus Quenched Anions

	Product Nitrate, mg/kg	Quenched Nitrate, mg/kg	Product Formate. mg/kg	Quenched Formate, mg/kg
RhRuHg1	30,300	27,660	61,900	61,900
RhRuHg2	28,900	31,100	60,700	65,000
RhRuHg10	28,400	30,300	62,900	62,800
RhRuHg4	27,400	28,400	61,800	62,300
RhRuHg5	31,200	30,600	62,800	65,200
RhRuHg6	30,900	28,100	72,800	62,200
RhRuHg7	29,200	27,600	61,400	59,100
RhRuHg8	28,600	28,200	57,700	56,400
RhRuHg9	26,500	28,300	61,200	61,300
RhRuHg11	27,600	27,600	58,200	58,400
RhRuHg12	28,800	27,600	59,100	57,800
RhRuHg13	28,100	27,900	59,100	58,600

The agreement for runs 8, 11, 12, and 13 (the later group of four runs) was excellent between the duplicate quenched sample result averages and the SRAT product sample result averages (all eight within 5%). There were some issues with the initial group of eight runs, and several SRAT product samples were reanalyzed (the initial RhRuHg1 formate was 73,000, but reanalysis showed 61,900). The two RhRuHg6 formate numbers differ by 17%, but most of the formate results compared very favorably between the two sample types. The RhRuHg6 product formate value analyzes as an outlier when compared to the other seven initial runs. The nitrate values are within 10% between the two sample types for a given run in the other set of eight runs. More often, product nitrate exceeded quenched sample nitrate indicating that nitrate destruction was probably not ongoing in the SRAT product sample. Product and quenched formate values split about equally as to which was higher indicating that formate destruction was not a major on-going reaction in the last half hour of the SRAT cycle.

Some ICP-Mass Spectroscopy (ICP-MS) data on the SRAT product slurry samples were obtained when certain hydrogen results were difficult to explain such as the three runs at midpoint trim loadings, Table 8. These noble metal compositions were probably harder to measure than the supernate noble metal concentrations reported in the bead-frit tests due to the lower concentrations in general and due to potential reduction of noble metals to the element

with plating out effects, general issues of sub-sampling heterogeneous slurries, etc. The insoluble noble metals had to be dissolved using aqua regia prior to analysis. Palladium was close to the detection limit of the instrument and showed considerable variation, even though it was targeted to the same concentration in all twelve runs. The two low Rh-low Ru combinations were not submitted, since the results were expected to be the most uncertain due to the low concentrations. RhRuHg4 was not submitted due to the corroding shaft issue.

Separate samples of SRAT product slurry were submitted for mercury analysis, Table 8. Issues with these samples also exist. Elemental mercury is not homogeneously distributed in the SRAT vessel at the end of the SRAT cycle, and it has been difficult to obtain representative samples in the past. Sub-sampling the SRAT product sample provides a second opportunity for obtaining a non-representative sample with respect to mercury. One column in the table indicates the targets for Rh, Ru, and Hg with H-L-L equivalent to high-low-low. These are for reference purposes.

Table 8. SRAT Product Noble Metals and Mercury

	Pd, mg/kg	Rh-Ru-Hg	Rh, mg/kg	Ru, mg/kg	Hg, mg/kg
RhRuHg1	n.a.	L-L-L	n.a.	n.a.	40
RhRuHg2	0.97	H-L-L	19	13	35
RhRuHg10	n.a.	L-H-L	n.a.	n.a.	440
RhRuHg4	n.a.	H-H-L	n.a.	n.a.	119
RhRuHg5	n.a.	L-L-H	n.a.	n.a.	53
RhRuHg6	0.46	H-L-H	20	19	475
RhRuHg7	<1	L-H-H	2.8	95	124
RhRuHg8	0.58	H-H-H	18	82	173
RhRuHg9	<0.9	M-M-M	9.4	60	242
RhRuHg11	1.0	M-M-M	9.1	56	87
H2Sim4	0.40	M-M-M	6.8	37	71
RhRuHg12 (2 rep)	0.86	H-L-L	25	19	212
RhRuHg13 (6 rep)	0.47	H-L-H	13	19	542

n.a. – not analyzed

Nominal midpoint SRAT product Rh would be about 18 mg/kg and midpoint Ru would be about 70 mg/kg. Low values should be about 1/3 midpoint (6 and 23, respectively) and high values should be about 5/3 midpoint (30 and 116, respectively). High Rh exceeds low Ru in concentration. The correct relative ranking was seen in RhRuHg2, RhRuHg6, and RhRuHg12, but not in RhRuHg13. Rh measured results were generally about 2/3 of the expected values, and Ru measured results were generally about 3/4 of the expected values.

H2Sim4 sample noble metal data was obtained for comparison to the two matrix midpoint runs in an attempt to explain the nearly three times higher hydrogen generation rates in H2Sim4. The Rh and Ru results were reasonably close to the two midpoint runs and were actually reported as slightly lower (fairly wide uncertainty), so the noble metal data do not explain the higher hydrogen generation results seen in H2Sim4. The two midpoint replicates in the matrix had

nearly a factor of three difference in the measured SRAT product mercury, with the run making less hydrogen also having less reported mercury (opposite of the expected effect).

Nominal Pd was 2.3 mg/kg. The measured palladium data were well below 2.3 mg/kg in all samples, but this was probably due to the small concentrations in the samples (barely above the detection limits) or due to plating out of Pd on the equipment. Each run had 0.0067 g of Pd in it compared to over 3000 g of trimmed slurry (about 0.00022% of the total mass), so it could easily get segregated from the bulk slurry and go undetected.

Agreement between measured noble metal results for RhRuHg2 and RhRuHg12 (replicate of 2) was fairly good, but the mercury results differed by a factor of six. Agreement between noble metal and mercury results for RhRuHg6 and RhRuHg13 (replicate of 6) was fairly good. In general, it was impossible to identify the high mercury runs from the low mercury runs using the SRAT product mercury analysis. The five low mercury runs ranged from 35-440 mg Hg/kg slurry, while the five high mercury runs ranged from 53-542 mg Hg/kg slurry. So 76% of the combined range of 35-542 was shared by the high and low mercury runs, even though they were a factor of five different in initial loading. Initial 0.5 wt% Hg was at about 1100 ppm. A product result of 35 ppm represents 97% stripping efficiency over 12 hours of reflux. This is more efficient stripping that expected based on historical data. The 53 ppm result in RhRuHg5 represents 99% stripping efficiency starting at 2.5 wt% Hg in just 24 hours. Pilot plant data prior to DWPF start-up did not support stripping efficiencies in the upper 90%'s after much longer reflux periods. Only single samples were submitted for each SRAT product slurry for the noble metals and mercury analyses. Many of these samples were actually prepared from a larger sample taken from the vessel at the end of the SRAT cycle rather than taken directly from the SRAT vessel. Consequently, there were two opportunities to obtain non-representative samples of the heterogeneous solids that were present in the SRAT before the sample was aliquoted for digestion by AD. This sample preparation methodology of consecutive sub-sampling is currently under review.

Solids and anion data were obtained on the six SME products. These data are given in Table 9.

Table 9. SME Product Anion and Solids Data

	Nitrate, mg/kg	Formate. mg/kg	Sulfate, mg/kg	Chloride, mg/kg	Wt % Total Solids	Wt % Insoluble Solids
RhRuHg1	27,700	64,900	n.a.	336	50.1	40.4
RhRuHg4	24,000	55,300	n.a.	424	50.7	41.2
RhRuHg5	27,900	67,600	n.a.	332	50.7	41.0
RhRuHg8	25,800	51,800	2160	476	50.4	41.1
RhRuHg9	26,400	61,200	n.a.	410	50.4	40.8
RhRuHg11	27,700	53,300	2300	386	49.7	42.2

n.a. – not analyzed

SME products were targeted to 50 wt% total solids, and all of the measured results were close to target. The RhRuHg11 samples had issues in the drying oven, so the wt% insoluble solids may

be overstated slightly or the wt% total solids may be understated slightly. There were actually more total supernate solids in the RhRuHg11 sample than in the RhRuHg8 sample (16.7% vs. 15.8%) even though the soluble solids worked out to 7.5% and 9.3% respectively on a % soluble solids per g slurry basis.

Snapshot samples were pulled during the SRAT cycle. Three samples were pulled each run. One sample was after dewatering, one was after six hours of reflux, and one was after eleven hours of reflux. These samples were centrifuged, and the supernate was analyzed for dissolved Rh, Ru, and formate (by ICP-AES and IC). The data were combined with the initial Hg loading and the DWPF equivalent hydrogen generation rate at the time of the sample. Statistical models were attempted to explain the hydrogen generation rates that included dissolved Rh, dissolved Ru, initial Hg, formate, and products of formate with both Rh and Ru. Data from RhRuHg2 and 4 were excluded (the bad shaft runs). Formate ion concentration was the only statistically significant factor to the instantaneous hydrogen generation rate that was found. Unfortunately there were analytical issues with the formate ion concentration data for the supernate samples (results approached and exceeded the amount of formate actually added in the first eight of the twelve runs; similar issues were present with the nitrate results which were 15-20% higher than indicated in the slurry samples).

Qualitatively, the supernate sample sets showed that the dissolved concentrations of Rh decreased with processing time after dewatering which corresponds to the behavior observed in previous runs. The dissolved concentration of Ru generally decreased from the end of dewatering until six hours into reflux, but it often steadied out and did not appear to fall further during the remainder of the SRAT cycle. There were some interesting observations with respect to Ru during the second half of reflux:

- RhRuHg1 and RhRuHg5 had increasing hydrogen generation from six to eleven hours into reflux and the dissolved Ru concentrations were steady during this period.
- RhRuHg10 and RhRuHg7 had increasing hydrogen generation from six to eleven hours into reflux and the dissolved Ru concentration fell.
- RhRuHg6, RhRuHg12, and RhRuHg13 had steady hydrogen generation from six to eleven hours into reflux and the dissolved Ru concentrations were also steady.
- RhRuHg4 hydrogen was falling and dissolved Ru concentrations were falling.
- RhRuHg9 and RhRuHg11 hydrogen generation was increasing slowly from six to eleven hours into reflux and the dissolved Ru concentrations rose slightly.

The data show some tendency for the instantaneous hydrogen generation rate to track the dissolved Ru concentration. There are uncertainties in the Ru measurements, but there were ten pairs of six hour-eleven hour Ru versus hydrogen to compare not counting the two runs with corroding shafts. In general these data confirm the statistical results that hydrogen generation and Ru are related later in the SRAT cycle, but these less specific results are targeted to the dissolved Ru rather than to the total Ru.

Qualitatively, the sample data showed that formate concentration changed little during reflux. Runs with higher than plausible measured formate concentrations (~100,000 mg/L) had similar results on all three samples from a given run (precision), and runs with plausible formate

concentrations also had similar results on all three samples (~75,000 mg/L) from a given run. The nearly constant formate concentrations and pH readings during reflux per run may have momentarily eliminated the speciation of formic acid between molecular formic acid and dissociated formic acid from the list of potential factors affecting hydrogen in this block of twelve runs. (The speciation probably was nearly constant under these conditions, whereas in runs where the pH rises significantly, the acidity of the formic acid decreases leading to more sodium formate relative to molecular formic acid.)

Supernate ICP-AES results were also obtained for dissolved Ca, Mg, and Mn from the above 36 samples. These three species changed the most of the major sludge species during reflux in the bead-frit runs. Results from the first four runs (RhRuHg1, 2, 10, and 4) and last four runs (RhRuHg8, 11, 12, and 13) indicated high extents of dissolution for all three elements throughout reflux consistent with the steady low pH readings. Results for the middle four runs (RhRuHg5, 6, 7, and 9) showed about 55-65% as much Mg and Mn dissolution relative to the other runs. Data for RhRuHg6 and RhRuHg9 were compared to their replicates, RhRuHg13 and RhRuHg11 respectively, and the lower extents of dissolution were not confirmed indicating a high likelihood of analytical issues with the ICP-AES supernate samples from the middle four runs (twelve samples analyzed as one block). Reduced extents of dissolution were also noted in the initial bead-frit matching run with 1.5 wt% mercury, and those results also appear to be suspect based on the timing of that run. There is no reliable indication in the Rh-Ru-Hg matrix study that mercury had a negative impact on the solubility of Mg and Mn at this acid stoichiometry.

Distribution:

J. C. Griffin, 773-A
D. A. Crowley, 999-W
C. C. Herman, 773-42A
A. B. Barnes, 999-W
B. J. Giddings, 786-5A
S. D. Fink, 773-A
D. J. McCabe, 773-42A
C. W. Gardner, 773-A

J. E. Occhipinti, 704-S
R. T. McNew, 704-27S
B. A. Davis, 704-27S
T. L. Fellinger, 704-26S
E. W. Holtzscheiter, 704-15S
J. M. Bricker, 704-27S
D. C. Sherburne, 704-S
H. H. Elder, 704-24S
J. F. Iaukea, 704-30S
J. W. Ray, 704-S

N. E. Bibler, 773-A
T. B. Edwards, 999-W
E. B. Fox, 999-2W
B. R. Pickenheim, 999-W
M. E. Stone, 999-W
R. E. Eibling, 999-W
D. P. Lambert, 999-W
J. M. Pareizs, 773-A
S. H. Reboul, 773-42A
C. J. Bannochie, 773-42A
J. D. Newell, 999-W
M. F. Williams, 999-1W
D. R. Best, 786-A